IEEE Access
Multidisciplinary | Rapid Review | Open Access Journal

Initial submission 25 August 2022, last revision 1 December 2022, accepted 15 December 2022, date of publication 21 December 2022, date of current version 3 January 2023.

Digital Object Identifier 10.1109/ACCESS.2022.3231481

RESEARCH ARTICLE

Approaching PetaVolts per Meter Plasmonics Using Structured Semiconductors

AAKASH AJIT SAHAI[1], MARK GOLKOWSKI[1], (Member, IEEE), THOMAS KATSOULEAS[2], (Fellow, IEEE), GERARD ANDONIAN[3], GLEN WHITE[4], CHANDRASHEKHAR JOSHI[5], PETER TABOREK[6], VIJAY HARID[1], (Member, IEEE), AND JOACHIM STOHR[4]

[1]Department of Electrical Engineering, University of Colorado Denver, Denver, CO 80204, USA
[2]Department of Electrical Engineering, University of Connecticut, Storrs, CT 06269, USA
[3]Department of Physics, University of California at Los Angeles, Los Angeles, CA 90095, USA
[4]Stanford Linear Accelerator Center, Menlo Park, CA 94025, USA
[5]Department of Electrical Engineering, University of California at Los Angeles, Los Angeles, CA 90095, USA
[6]Department of Physics, University of California at Irvine, Irvine, CA 92697, USA

Corresponding author: Aakash Ajit Sahai (aakash.sahai@gmail.com)

This work was supported in part by the Department of Electrical Engineering, University of Colorado Denver; The simulations were supported by the NSF Extreme Science and Engineering Discovery Environment (XSEDE) Rocky Mountain Advanced Computing Consortium (RMACC) Summit Supercomputer funded by the NSF under Award ACI-1548562, Award ACI-1532235, and Award ACI-1532236; in part by the University of Colorado Boulder; and in part by the Colorado State University [20], [21].

ABSTRACT A newly uncovered class of plasmons in the strongly excited limit opens access to unprecedented Petavolts per meter electromagnetic fields with wide-ranging, transformative impact. Unlike conventional plasmons, such plasmons are constituted by non-perturbative, large-amplitude oscillations of the ultradense, delocalized free electron Fermi gas inherent in conductive media. Here structured semiconductors doped to have an appropriate conduction electron density are introduced to tune the properties of the Fermi gas for matched excitation of large-amplitude plasmons using readily available electron beams which enables immediate experimental validation. Specifically, an electrostatic, surface ''crunch-in'' plasmon is collisionlessly excited by the beam launched inside a tube. Strong excitation due to matching results in relativistic oscillations of the electron gas and unravels unique phenomena. Relativistically induced ballistic electron transport comes about due to relativistic multifold increase in the mean free path and also leads to unconventional heat deposition beyond Ohm's law. This explains the absence of observed damage or solid-plasma formation in past experiments on conductive samples interacting with electron bunches shorter than 10^{-13} seconds. Furthermore, relativistic momentum leads to copious tunneling of electron gas across the surface, which then crunches inside the tube. Relativistic effects along with large, localized electron density variations underlying these modes necessitate kinetic approach to theoretical and computational modeling. Kinetic model presented here demonstrates experimental viability of observing tens of gigavolts per meter plasmonic fields excited by matching readily available electron beams to plasmons in semiconductors with 10^{18}cm^{-3} free electron density, and paves the way for Petavolts per meter plasmonics.

INDEX TERMS Plasmons, surface plasmon, nanoscience, electromagnetic field theory.

I. INTRODUCTION

Plasmons are quasi-particles that are constituted by modes of collective oscillations of free electron Fermi gas which is a quantum-mechanical entity inherent in conductive media [1], [2]. The electron gas itself exists because of the periodic ionic lattice which engenders distinct electron energy bands in adherence with Bloch's theorem [3]. Only the electrons that occupy the conduction band comprise the Fermi gas that is delocalized and free to move about the entire lattice when externally excited. Beside the composition and structure of the ionic lattice, numerous quantum effects work in unison to

The associate editor coordinating the review of this manuscript and approving it for publication was Gokhan Apaydin.

bring about the highest, at equilibrium terrestrial density of Fermi electron gas. For instance, metals can have an equilibrium free electron Fermi gas as dense as $n_0 \simeq 10^{24}\text{cm}^{-3}$.

Nano-electromagnetic phenomena that allow nanoscale control over electromagnetic (EM) energy are made possible by this ultra-high electron density which constrains the size or wavelength of plasmons as,

$$\lambda_{\text{plasmon}} = 33\ (n_0[10^{24}\text{cm}^{-3}])^{-1/2}\ \text{nm}. \quad (1)$$

The ability to nanometrically confine EM energy has resulted in a wide-range of breakthroughs using perturbatively excited optical plasmonics [4]. Perturbative plasmons excited by electron microscopy beams have also enhanced imaging at the angstrom level [5].

Our work [6], [7], [8] has laid the foundation of a new physical model of strongly excited plasmons. Strongly excited plasmonics is characterized by the spatial amplitude of collective electron oscillations, δ approaching the plasmonic wavelength, $\delta \simeq \lambda_{\text{plasmon}}$. However, the ionic lattice is not disrupted. These non-perturbative or large-amplitude plasmons [6], [7] are electrostatic due to large-scale electron density displacement $\Delta n_e \simeq n_0$, in contrast with conventional plasmons. The ultimate strength of nonlinear oscillations of free electron Fermi gas is limited by breakdown in coherence. This coherence limit of plasmonic EM fields is put forth in our model to be at least of the order of the so-called ''wavebreaking'' limit [9] in plasmas,

$$\text{E}_\text{p} = \frac{m_e c^2}{e}\frac{2\pi}{\lambda_{\text{plasmon}}} \simeq 0.1\sqrt{n_0[10^{24}\text{cm}^{-3}]}\text{PVm}^{-1}. \quad (2)$$

Accordingly, electrostatic plasmons with large-amplitude oscillations of the ultradense, 10^{24}cm^{-3} electron gas can open access to unprecedented Petavolts per meter fields. These PV/m fields are accessible with techniques such as plasmonic nanofocusing [10] of charged particle beams propagating inside tapered tubes, to ultrasolid densities.

Access to EM fields that are many orders of magnitude higher than other known techniques makes it possible to directly access frontier physics such as ''opening the vacuum'' and ''probing the quantum gravity fabric of spacetime'' discussed in sec.II. Furthermore, apart from various technological applications [8], PV/m fields and ultrasolid beams open transformative possibilities for future particle colliders.

The physics of PV/m plasmonics has not been previously studied which sets apart this work [6], [7]. PV/m plasmonics has become practicable with the uncovering of an electrostatic surface plasmon that can be excited with quasi-solid particle beams of sub-micron dimensions that have been recently modeled to be feasible.

In this work, specifically, semiconductor plasmons are introduced and demonstrated to enable immediate prototyping. The tunability of electron gas in semiconductors enables matching of the properties of plasmons with existing particle beams which is essential to excite large amplitude plasmons. As the large amplitude plasmon model breaks away from existing directions in plasmonics, a key objective is also to set the ''tunable plasmon'' model within the framework of its freshly introduced foundational principles through a brief review. Towards this objective, plasmonics is carefully reviewed and disambiguated from modes in other media, namely dielectrics (insulators) and plasmas (gasses).

A. BACKGROUND: LARGE-AMPLITUDE PLASMONS IN METALLIC NANOMATERIALS

The original work [6], [7] introduced large-amplitude or nonlinear, relativistic plasmons that are collisionlessly excited by the collective fields of charged particle beams propagating inside the hollow region of a tube. Large-amplitude plasmons are most effectively excited by ultrashort particle beams. Direct excitation of such plasmons using optical photons ($\lambda_0 > 400$nm) is challenging because their size in typical metals, per Eq.1 is significantly smaller.

More importantly, incoherent energy unavoidably present in the pre-pulse of high-intensity optical lasers ablates the ionic lattice and irreversibly disrupts the electron gas. Due to heating by optical energy in the pre-pulse over nanoseconds the ionic lattice breaks down into randomized ion gas, converting the plasmonic system to plasma.

As long as the ionic lattice exists, all atomic electrons of conductive condensed matter systems occupy either the valence (bound) or the conduction (free) energy band. Note that the ions are many orders of magnitude heavier than electrons and therefore, the ionic lattice is only weakly perturbed over a few periods of plasmonic oscillations. The conduction band population that exists at equilibrium in accordance with Bloch's theorem without any external excitation can be engineered to tune the properties of plasmons. Essentially, the degenerate quantum gas of fermions (ionic lattice) which is critical for plasmons is absent in dielectrics and stands in stark contrast with classical electron gas (ion gas) in absence of any ionic structure in plasmas (detailed in sec.III).

Using tunable properties of conductive materials, large-amplitude, electrostatic surface plasmons were first modeled in [6] by launching an upcoming hundreds of pico-Coulomb (pC) relativistic electron bunch of sub-micron dimensions [11], [12] (detailed in sec.VI) inside a tube. The predominantly radial ''pancake'' collective fields of the relativistic beam excite a surface plasmon and make it possible to overcome disruptive instabilities that dominate collision mediated interactions in bulk media.

However, modeling large amplitude plasmons is quite challenging because material properties such as permittivity that hardly diverge from their initial macroscopic average in the perturbative limit have large-scale, highly localized microscopic variations in the nonlinear limit. A kinetic approach coupled with particle-tracking simulations (discussed in sec.IV-A) is therefore introduced in our work for modeling large amplitude plasmons. Specifically, the new physical principle of relativistically induced ballistic transport [6] introduced in our work makes collisionless particle codes suitable for modeling large amplitude plasmons.

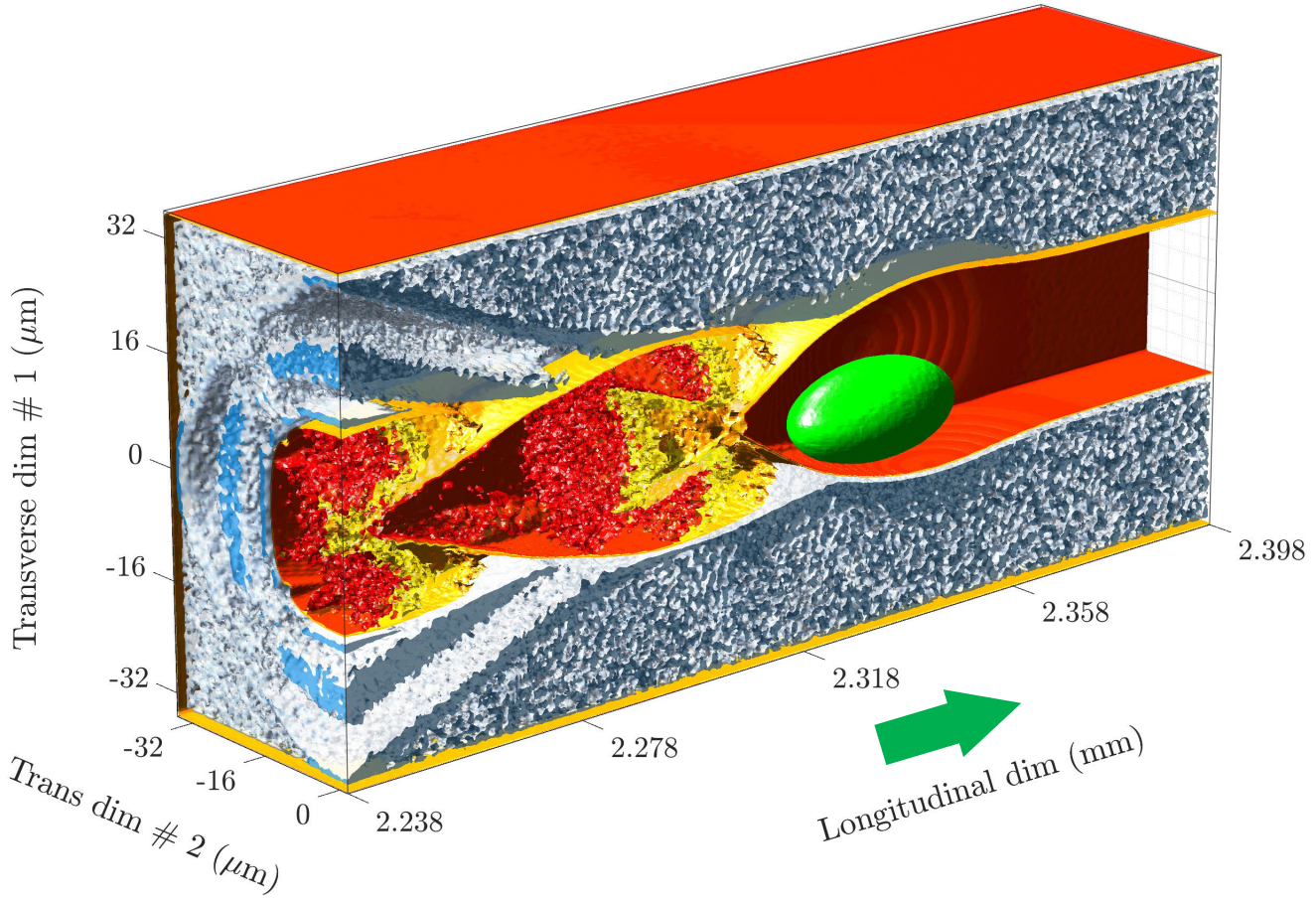

FIGURE 1. Representation of electron gas density profile of semiconductor-based surface "crunch-in" plasmonic mode excited by a relativistic electron beam (in green) with initial dimensions $\sigma_{z,r} \sim 10\mu$m propagating (to the right) inside a n-type doped Silicon tube of $25 \times 25\mu\text{m}^2$ rectangular cross-section and 10^{18}cm^{-3} conduction band electron density. This is a snapshot at 2.4 mm (~ 8ps) of sustained interaction modeled using a three-dimensional (3D) particle-in-cell code.

In our particle-tracking based computational model, a tube with nanoengineered wall of free electron Fermi gas density $n_t = 2 \times 10^{22}\text{cm}^{-3}$ was verified to sustain surface "crunch-in" plasmon [13], [14], [15] (where relativistically excited free electrons traverse the surface) with tens of TV/m fields in accordance with Eq.2.

The surface crunch-in plasmon is found to be significantly different from the conventional, purely electromagnetic surface plasmons that are transverse magnetic (TM) [16]. While the TM surface plasmon is sustained by perturbative surface electron oscillations, relativistically excited electrons underlying surface crunch-in plasmon oscillate across the tube surface and crunch inwards towards the tube axis. Focusing fields of this non-TM, nonlinear surface plasmon also enable guiding the beam through the hollow core of the tube.

Effective excitation of large-amplitude plasmons requires that the dimensions of the beam $(\sigma_\text{r}, \sigma_\text{z})$ approach those of the plasmon. In [6], wall density n_t and tube radius $r_t = 100$nm were chosen for a surface plasmon wavelength of $\lambda_\text{plasmon} \simeq 250$nm. The dimensions of the electrostatic surface plasmon were thus matched to the sub-micron nanoCoulomb electron beam of bunch length $\sigma_\text{z} = 400$nm [11] and waist-size $\sigma_\text{r} = 250$nm [12]. Large collective fields of such dense beams, $n_b \gtrsim 10^{20}\text{cm}^{-3}$ impart relativistic momentum $\gamma_\text{plasmon}\beta_\text{plasmon}m_e c$, to the free electron Fermi gas which relativistically elongates the plasmon dimensions $\gamma_\text{plasmon}\lambda_\text{plasmon}$ ($\beta_\text{plasmon} \simeq 1$) and enhances the match.

However, this combination of bunch charge and dimensions is only likely to be available in the near future.

B. TUNABLE PLASMONS USING SEMICONDUCTORS

In this work, to promptly prototype large amplitude plasmons, structured semiconductors are introduced and modeled to sustain large amplitude, electrostatic surface plasmons using a present day beam. The free electron Fermi gas density in semiconductors can be widely tuned by appropriately choosing the type and concentration of dopant atom embedded in the ionic lattice. Extrinsic semiconductors up to the limit of degeneracy [17] have a tunable conduction band electron density between 10^{13-21}cm^{-3} and a corresponding plasmonic wavelength using Eq.1,

$$\lambda_\text{plasmon} = 3.3\ (n_0[10^{20}\text{cm}^{-3}])^{-1/2}\ \mu\text{m}. \tag{3}$$

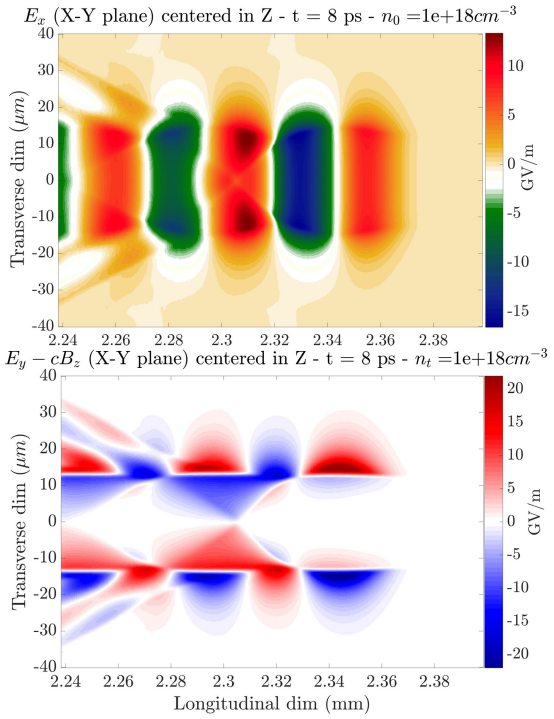

FIGURE 2. Cross-sections of the accelerating (top panel) and focusing (bottom panel) field profile of the semiconductor-based surface crunch-in plasmon in Fig.1.

Semiconductor plasmons are thus highly tunable and allow spatiotemporal match with readily available particle beams. By deploying suitably doped semiconductors it becomes possible to immediately prototype and determine the principles underlying electrostatic plasmons that enable PV/m plasmonics. Specifically, n-type extrinsic semiconductors of appropriately doped free electron concentration which allow control over spatial dimensions of plasmons are demonstrated to match with ten micron electron beam. For proof of this principle, one such currently accessible electron beam used in our model is described further in sec.IV-B. It is also of interest to note that perturbative semiconductor plasmonics [18] is an active area of research.

However, the operating bunch length for PV/m plasmonics is ideally limited to less than a few tens of micron to avoid affecting the ionic lattice during or after the interaction. In particular, experiments [19] have reported absence of damage or solid plasma formation in conductive samples upon interaction with bunches shorter than 10^{-13}sec (see sec.III-A).

Proof of concept of matched excitation of large-amplitude semiconductor surface crunch-in plasmon using readily accessible electron beam is furnished using three-dimensional (3D) kinetic computational model based upon highly parallelized particle-in-cell (PIC) simulation carried out using several thousands of cores of the NSF XSEDE RMACC Summit supercomputer [20], [21]. Fig.1 shows the contours of density profile of the electron gas to elucidate the mode. The semiconductor tube has a square cross-section of 25μm $\times$ 25μm and doped to have equilibrium conduction band electron density of $n_t = 10^{18}\text{cm}^{-3}$. This tube is excited by launching a currently accessible relativistic ($\gamma_b \sim 10^4$) nC electron beam with dimensions, $\sigma_{z,r} = 5\mu$m. It is also noted that this is the first model of surface crunch-in plasmon in a rectangular tube. The field profile, longitudinal (top) and focusing (bottom), of the electrostatic, surface crunch-in plasmon excited in the semiconductor tube is presented in Fig.2. Note that, because PIC simulations are not required for perturbatively exited plasmons, their early adoption by our work here does not fully take into account all the condensed matter effects. Details of the methodology and simulation setup in open-source EPOCH code [22] are in sec.IV-A.

Large amplitude excitation is evident from Fig.1 with the foray of tube electron trajectories inside the tube corresponding to an amplitude of $\delta \simeq 25\mu$m (= tube radius). Therefore, the trajectory amplitude δ is a significant fraction of $\lambda_{\text{plasmon}}[10^{18}\text{cm}^{-3}] = 33\mu$m. The tens of GV/m plasmonic fields sustained in 10^{18}cm^{-3} semiconductor tube in Fig.2 are at the lower end of plasmonic reach. However, even at the lower end experimental investigations stand to unravel the underlying principles of these unexplored modes. Specifically, relativistic momentum acquired by the electron gas under matched excitation leads to the emergence of new phenomena. Plasmonic dynamics is significantly modified in addition to relativistic elongation, noted above.

Large-amplitude processes of free electron Fermi gas oscillations uncovered in our model [6], such as relativistically induced ballistic electron transport and relativistic ultrafast electron tunneling (described in III-D) begin to dominate the plasmonic dynamics. These effects further diverge from conventional plasmonics. In addition to the non-perturbative approach due to nonlinearity where spatiotemporally averaged macroscopic material properties are ineffective, these new phenomena necessitate the kinetic approach. The kinetic approach makes it possible to account for relativistic momentum and large scale local accumulation of particles which engenders spatially dependent constitutive properties.

This large amplitude semiconductor plasmon effort based on matched excitation using ten micron electron beam is also computationally contrasted against dielectric and metallic tube. This helps immediate experimental verification and delineation of the underlying principles and further bolsters the framework of PV/m plasmonics.

C. ORGANIZATION OF SECTIONS

In sec.II non-collider possibilities to directly access frontiers of fundamental science using PV/m plasmonic fields are briefly described. Framework of large amplitude plasmonics excited by dense particle beams is elucidated in sec.III, as follows: key enabling advances that make this initiative technologically practicable now in III-A, characteristics of free electron Fermi gas in III-B, higher order effects in the presence of ionic lattice in III-C, new phenomena due to relativistically oscillating free electron Fermi gas in III-D, dis-

ambiguation from dielectrics, optical plasmons and plasma based techniques in III-E, comparison of electrostatic surface modes against conventional electromagnetic surface mode in III-F, selected analytical results in III-G and dynamic aperture of surface crunch-in modes in III-H.

In sec.IV-A, kinetic modeling approach and details of the simulation setup are described. Phase-space of a currently available ten micron, nC relativistic electron beam which is used in our model is summarized in sec.IV-B. By porting this beam phase-space from beamline simulations into our plasmonic PIC simulations, effect of large amplitude semiconductor plasmons is estimated with: properties of plasmons excited in different tube dimensions in sec.IV-C and the effect of plasmonic fields on beam transverse phase-space and energy spectra in sec.IV-D. Besides estimation of experimental signatures of the fields of semiconductor plasmons on the beam, semiconductor plasmons are contrasted against plasmons excited by the same beam in metallic tube used in [6] in sec.IV-E. The ongoing sample fabrication efforts are also outlined in sec.V.

Although the proof-of-principle described here utilizes semiconductor plasmons to match with readily available tens of micron beams, attaining ultimate limits of PV/m plasmonics aligns with the ongoing efforts on Mega-Ampere peak current beams discussed in sec.VI. This includes compression of nC particle bunches to sub-micron dimensions, bunch length in VI-A and waist-size in VI-B.

II. FRONTIER FUNDAMENTAL SCIENCE USING PV/M PLASMONIC FIELDS

PV/m plasmonic fields open new pathways in fundamental science. In the near-term PV/m fields open the possibility of non-collider examinations of frontier fundamental science. Below we summarize two such selected searches at the limits of current explorations that exemplify the possibilities.

On the other hand, using PV/m fields for particle acceleration opens up ultra-compact particle colliders accessing PeV particle energies using meter-scale machines. Besides drastic reduction in machine size, solid density beams naturally increase the rate of direct collision between particles and open a new paradigm for luminosity which defines event rates in colliders. Solid-based accelerators provide a more direct path to multi-stage machines and being hollow are suitable for positron acceleration and collisional emittance (phase-space volume of the beam) preservation.

A. OPENING THE VACUUM WITH PLASMONIC FIELDS: NONLINEAR QUANTUM ELECTRO-DYNAMICS (QED)

In the non-perturbative limit of QED theory, the rate of spontaneous production of positron-electron pairs directly off the vacuum increases under extreme electromagnetic fields that approach the Schwinger field limit of $E_s = 1.3 \times 10^{18} V/m$ [23]. This rate increases exponentially with the electric field E_{lab} as $\exp(-\frac{\pi m_e^2}{eE_{lab}})$ as is typical of tunneling effects.

Plasmonic fields allow nearing the EV/m Schwinger field limit and help direct observation of ''opening the vacuum''. Access to extreme fields is based upon the use of plasmonic fields to nano-focus particles beams [10]. Plasmonic nanofocusing increases the electric field of particle beams similar to the well known effect in optical plasmonics where tubes with longitudinally tapered radius are used to nano-focus the EM energy coupled into optical plasmons [24].

While other schemes have been proposed to experimentally examine high-field breakdown of vacuum, such as colliding two high-intensity laser pulses or the collision of an ultra-relativistic particle beam with an intense laser pulse, PV/m plasmonics offers numerous advantages. Electromagnetic fields sustained by plasmons have a near-zero group velocity and are localized in space. So, plasmonic fields:

- do not travel with the particle or laser beams, or
- need not exist only in a Lorentz-boosted frame, or
- do not exist only momentarily at a collision point

These unique advantages motivate PV/m plasmonics as an attractive alternative to examine nonlinear QED without a collider. Non-collider beams do not have a stringent requirement on their emittance or energy spread and can therefore be utilized for fundamental science.

B. PROBING THE FABRIC OF SPACETIME: QUANTUM-GRAVITY MODEL WITH ULTRAENERGETIC PHOTONS

Theories that attempt to describe gravity using a quantum mechanical framework as well as theory of everything models are considered to be examinable only using astrophysical observation data.

One of predictions of the string theoretical model that is considered to be verifiable only using astrophysical radiation sources is the non-trivial permittivity to ultra-energetic photons exhibited by vacuum [25]. With the nature of interaction between short wavelength photons and the vacuum, the most appropriate probes of this model are bursty astrophysical sources that produce short pulses of ultra-energetic photons. Therefore, detection of these effects is sorely dependent on observational data.

PV/m plasmonics opens the possibility of bursty TeV or PeV photon production using the nano-wiggler mechanism [6]. A nano-wiggler utilizes the extreme focusing fields of plasmons to wiggle the ultrarelativistic electrons of a non-collider beam (low particle count, relatively large emittance and energy spread) that have a relativistic factor, $\gamma_b \simeq 10^{4-7}$. Nanometric wiggling oscillations wavelengths, λ_{osc} produce photons of energy, $2\gamma_b^2\, hc/\lambda_{osc}$ ranging from tens of GeV to TeV. Beam particles under the action of PV/m plasmonic fields can thus produce quasi-coherent photons of unprecedented energies.

Therefore, access to unprecedented ultra-energetic photons using the nano-wiggler mechanism opens the possibility of examining the predictions of quantum gravity model.

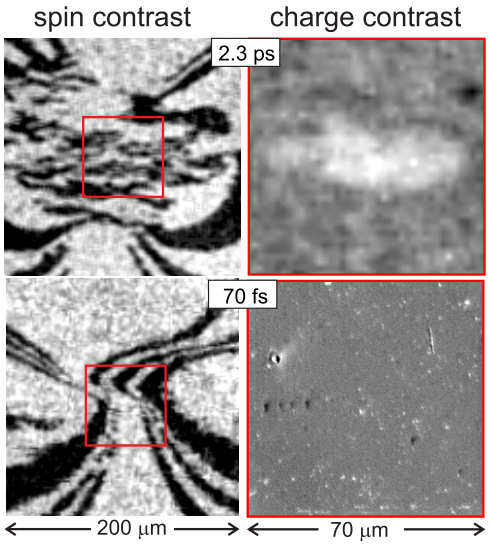

FIGURE 3. A comparison of the sample images obtained with Scanning Electron Microscope (SEM) with spin polarization (SEMPA), on the left, and conventional SEM of the sample, on the right, zoomed in on the region where the beam hit. It is evident that for electron bunches shorter than $\sigma_{\parallel} \leq$ 100fs there is no topological deformation or solid-plasma formation.

III. PV/M PLASMONICS FRAMEWORK

A. KEY ENABLERS OF PV/M PLASMONICS

Two key experimental advances underpin practical considerations behind the PV/m plasmonics effort:

1) **No experimentally observed damage, plasma formation or large-scale ionization of conductive samples for shorter than** 20μm **long electron bunch:** Firstly, ultrafast magnetic switching experiments [19] observed no damage or plasma formation on a many millimeters-thick conductive magnetized Iron-Cobalt alloy sample using transmission electron microscopy (TEM) after its interaction with a few nC, less than 100fs long, tens of micron waist electron beam. Although no damage was detected using charge-contrast TEM, spin contrast TEM revealed that electron spins had switched over these ultrashort timescales. The magnetic stripes leftover after the interaction indicate strong coupling from the beam fields to the magnetic domains in the sample and it heating above a critical temperature. In contrast, severe damage was observed along with magnetic switching when the same sample interacted with a 2.3 picosecond long electron beam [26].
   Fig.3 shows a comparison of material damage for the two field pulses of different length and field strength illustrated using spin sensitive transmission electron microscopy in Fig.3(a) and conventional transmission electron microscopy in Fig.3(b).
   The relativistic plasmonic model of large-amplitude modes offers an explanation for this fascinating observation that still remains unexplained. Upon compression of the bunch with nC charge from 2.3ps to 70fs while the waist-size remains the same, the electric field increases by a factor of 33. This orders of magnitude increase in the beam electric field makes the plasmonic oscillations more relativistic making them ballistic and consequently modifies the heat deposition mechanism. Relativistically augmented mean free path of the Fermi gas do not result in collisional deposition of heat and cannot be explained using the Ohm's law.
   The onset of ballistic heat transport by relativistic free electron Fermi gas therefore eliminates the formation of solid-plasma during or after the interaction. This ensures that when a dense charged particle beam less than $\leq 10^{-13}$sec long induces relativistic oscillations, plasmonic effects dominate and there is no sample damage.
2) **Extreme bunch compression**: Secondly, rapid and ongoing technological innovations have now made it possible to compress a charged particle beam containing 10^{10} particles to sub-micron overall dimensions. Recent beamline simulations [11] have demonstrated that a nC electron beam can be compressed to 100nm bunch length [12]. Similarly, magnetic lens based focusing systems are being prototyped to compress the beam waist-size to hundreds of nm. Effort towards MegaAmpere peak current beams with sub-micron waist sizes is summarized in sec.VI.

B. FREE ELECTRON FERMI GAS: A QUANTUM ENTITY

The free electron Fermi gas is governed by several key quantum mechanical effects. Periodic structure of the ionic lattice as well as the nature of inter-atomic bonding due to the overlap of orbitals of neighboring atoms is critical to the existence of the Fermi electron gas. Potential of the periodic lattice confines orbital electronic wave-functions such that distinct electronic energy bands are formed in accordance with Bloch's theorem [3]. Energy bands are near-continuum levels of electron energy states that although themselves partitioned by an infinitesimal quanta of energy, are separated from other bands by a substantial forbidden energy gap.

In conductive materials, the conduction band contains a dense gas of free electrons that are not tied to any specific atom in the lattice. In particular, electrons that occupy energy states in the conduction band constitute a free electron gas which follows the Fermi-Dirac statistics. The Pauli's exclusion principle [27] forbids electron-electron interaction making it possible to form an ultra-dense quantum gas of non-interacting Fermions.

The Fermi electron gas freely moves about the entire lattice. Upon external excitation, it undergoes collective oscillations [1]. Over plasmonic timescales the structure of the ionic lattice may get distorted but does not get disrupted. In our work the electron gas is driven to its coherence limit and sustains extreme collective fields which form the basis of PV/m plasmonics.

C. IONIC LATTICE AND INTERBAND TRANSITIONS

The ultrashort particle beams (less than 100 femtoseconds) suitable for PV/m plasmonics is considerably shorter than the timescale of ion motion. So, the ionic lattice as well as the energy bands exist over the timescales of existence of plasmons. Therefore, plasmons dominate the interaction.

However, higher order effects under the action of intense fields such as interband transition of the valence band electrons to the conduction band, changes in the band structure due to lattice distortion or phonon oscillations etc. will have to be taken into account.

The interband transition rate is estimated taking into account the frequency content of the EM pulse (coherent and incoherent content) created by the particle bunch. The method of virtual photons or Weizsacker-Williams method [28], [29] is used to calculate the field of virtual photon bunch with equivalent frequency components. The half-cycle unipolar EM pulse equivalent to the particle bunch does have a direct current component which however plays no role in estimation of interband transitions. The bunch of virtual photons converts to that of real photons upon interaction of the particle bunch with an external particle or field.

The ten micron long ($\leq 10^{-13}$ second) bunches of our work have a coherent virtual photon frequency spectrum which is restricted to few tens of THz with the bunch length being comparable to THz wavelengths. The equivalent photon energy (tens of milli eV) of THz wavelengths are well below the interband transition energy in most conductive solids. Therefore, bulk transition is not a possibility. Such transitions may occur in spatially localized regions of high peak plasmonic fields. However, high-field transitions effectively inject these electrons into the plasmonic fields and create a new population within the electron beam.

So, in this work interband transitions and other higher-order effects are safely neglected. However, in the future when bunch lengths approach submicron dimensions as discussed in sec.VI and the beam field increases, our modeling will incorporate high-order effects.

D. NEW EFFECTS IN LARGE-AMPLITUDE PLASMONICS

Relativistically induced ballistic transport: In perturbative plasmonics, oscillations are collisionless because the oscillation amplitude is much smaller than plasmon wavelength $\delta \ll \lambda_{\text{plasmon}}$ as well as the mean free path $\delta < \ell_{\text{mfp}}$. In the original work in [6], increase in the mean free path with increasing free electron momentum, $\ell_{\text{mfp}} \propto p_e$ was identified as a key effect underlying large amplitude plasmonics.

The mode of free electron transport in conductive media transitions from the usual Ohmic to ballistic [30] as ℓ_{mfp} becomes longer than the thickness of the media. Under ballistic condition, the free electron gas has negligible collisions or scattering with impurities and resultantly the Ohm's law does not apply. It is important to note that, in general, classical transport of carriers is considered under continuously applied external electric field (in the form of terminal voltage) which results in net or average transport of the free electron Fermi gas across a conductive media between the electrodes.

However, electron transport in plasmonic oscillations is excited by electromagnetic pulses without any direct external injection of electrons from an electrical contact. Therefore, average electron transport in oscillatory motion is spatially limited to the order of plasmonic wavelength of the specific underlying media. Being perturbative the oscillation velocity in conventional plasmons still remains very close to the Fermi velocity, $v_F \simeq 0.01c$.

When large amplitude oscillations are excited such that the Fermi gas electrons gain relativistic momentum, these relativistically oscillating electrons acquire induced ballistic character. As relativistic plasmonic modes have not been previously studied, our work uncovers and finds this effect to be quite critical for large amplitude plasmonic dynamics. Specifically, for electrons of the Fermi gas oscillating with an average Lorentz factor of $\langle\gamma_e\rangle$, the relativistic mean free path increases as $\langle\gamma_e\rangle^k \times \ell_{\text{mfp}}$ where, k is a scaling factor which depends upon the material and other related factors.

This relativistically induced multifold increase is also experimentally observed with externally incident electron beams and is interpreted to be due to significant reduction in interaction length of electron with an ionic center in the lattice. Typically, the interaction cross-section $\sigma \propto \ell_{\text{mfp}}^{-1} \propto \langle\gamma_e\rangle^{-k}$, scales as $\sigma \propto \mathcal{E}^{-2}$ with particle energy $\mathcal{E}$. Therefore, ℓ_{mfp} would at least scale as γ_e^2.

The relativistic ballistic transport model is rooted in the experimental observation of no damage as the beam fields increase with bunch compression from 2.3ps to 70fs, discussed in sec.III-A.1. With a 33 times increase in the beam fields which correspondingly increases the relativistic factor $\langle\gamma_e\rangle$ of the oscillating free electron gas in experiments, $\ell_{\text{mfp}}(\gamma_e)$ is expected to increase by a factor of at least 10^3.

Relativistically elongated mean free path resulting in an increase of 1000 times compared to the Fermi gas at equilibrium, transform the dynamics of free electron gas including heat transport well beyond Ohm's law.

Relativistic tunneling of electron gas which traverses the surface potential: Another key effect identified in [6] is the increase in the probability of ultrafast tunneling across the surface potential under relativistic excitation. The conduction band electrons in metal are capable of tunneling through the surface potential [31]. Especially those electrons with velocities that lie in the tail of the Fermi-Dirac distribution function and whose energy approaches the barrier potential. The rate of tunneling, a near-instantaneous process, depends on particle energy relative to the barrier potential.

In perturbative plasmonics, energy of nearly the entire distribution of the excited free electron gas is much smaller than the surface potential. So, tunneling is minimal and inconsequential to the dynamics if at all present. However, in large amplitude plasmonics as the electrons are driven to relativistic velocities they become capable of tunneling through the surface, in both directions. This is in addition to their ''above

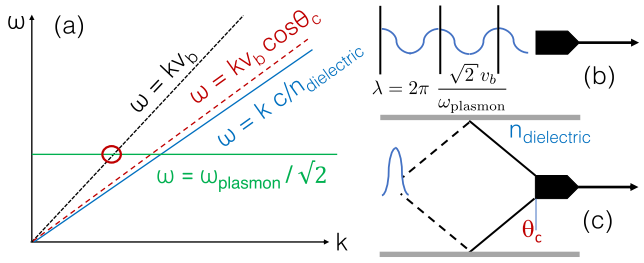

FIGURE 4. Dispersion relation for surface plasmon and dielectric modes in (a) and their overlap with the excitation pulse which determines the spatial and temporal profile, (b) of the surface plasmon mode, (c) of the dielectric mode.

the barrier" free propagation when their oscillation energy exceeds the surface potential.

Particularly, as the free electrons are primarily driven transverse to the tube axis, even weakly relativistic oscillations freely oscillate across the surface. It is important to note that being near-instantaneous, relativistic tunneling across the surface is critical to the dynamics of large-amplitude plasmons.

E. DISAMBIGUATION FROM OTHER MECHANISMS

1) **Dielectric or insulating solids**: Dielectrics or insulating materials have near zero electron density in the conduction band. Although there appear to be phenomenological similarities between the plasmons in conductive media and the electromagnetic modes in an insulting dielectric because both use a hollow solid tube, the physics of each is quite distinct.
Whereas plasmonic modes are supported by collective oscillations of free electron Fermi gas, dielectric modes are supported by polarization currents generated by the distortion of the electron cloud bound to the ions in the lattice. Plasmonic oscillations are out of phase with the excitation electric field (or oppose the fields of the excitation) while dielectric polarization currents are not. In dielectrics, polarization currents excite Cherenkov radiation which supports the acceleration mechanism. In large-amplitude plasmonics, electrostatic plasmons supported by large-scale charge separation between the free electron Fermi gas and ionic lattice sustain ultra-high gradients.
As a result, the dispersion relation of each type of wave is quite different:
   - $\omega = \frac{\omega_{\text{plasmon}}}{\sqrt{2}} = \sqrt{\frac{4\pi n_0 e^2}{2m_e}}$ for a surface plasmon,
   - $\omega = k\ c/n_{\text{d}}$ for a dielectric wave, where n_{d} is the index of refraction of the dielectric.

   The resulting mode structure can be predicted from the intersection of the dispersion relations and the driver disturbance at $\omega = kv_b$ (where, $v_b = c\beta_b$ is the beam velocity) shown in Fig.4a. From this we see that the surface plasmon has but one wavenumber and frequency which gives rise to planar wave fronts and sinusoidal oscillations as in Fig.4b.
   On the other hand, the dielectric dispersion intersects the beam disturbance at the Cherenkov angle $cos(\theta_c) = 1/n_{\text{d}}$ at every ω and k. This supports the familiar Cherenkov cone type wavefront structure common in the wake of supersonic jets and illustrated in Fig.4c. This shock-like cone propagates out to the outer conducting wall boundary of the dielectric whereupon it is reflected back toward the axis, giving rise to an accelerating spike on the axis as in Fig.4c. In order to sustain fields in dielectrics, it is critical to trap the Cherenkov radiation using an outer metallic wall. In the absence of an outer metallic wall, the Cherenkov radiation is dissipated outwards away from the tube.
   It is clear from this that the modes in conductive and dielectric solids considerably differ. In the first, the accelerating field is nominally sinusoidal (when linear) and the spatial location of the peak field behind the excitation is controlled by the free electron Fermi gas density in the tube. In the second, the accelerating field is a single spike and its location is determined by the outer radius defined by metallic deposit and the dielectric constant of the tube.
   Experiments have demonstrated that in a dielectric when the bound electrons are freed up by EM fields of intense Cherenkov radiation to transition into the empty conduction band of the dielectric, the electromagnetic wave is rapidly shielded and damped by these free electrons which puts an end to any action of the dielectric fields [32].
   While dielectric effects are important when electromagnetic waves interact with a media, electrostatic plasmons where effects of charge-separation dominate over electromagnetic wave are not affected by dielectric properties of the media.
2) **Optical plasmons**: In conventional plasmonics, optical femtosecond laser is used to excite weakly-driven plasmons. Such optical plasmons that have also been proposed as a pathway for particle acceleration [33] are perturbative unlike in our work.
3) **Solid plasmas and crystal channeling**: Solid plasmas do not exist at equilibrium and are created by ablation of solids such as by heating the solid with a high-intensity optical (near-infrared) laser.
   In solid plasmas the individual ions are uncorrelated (ion gas) as there is no ionic lattice. Consequently, solid plasmas do not have an energy band structure. Due to the highly randomized nature of ions in plasmas, the properties of plasma oscillations significantly diverge from that of plasmons especially at higher densities.
   The individual atoms that have to be ionized to form a plasma result in an electron density that solely depends on the atomic density and the ionization fraction. Also, electron-electron collisions which increase with electron density in a gaseous plasmas are minimized for a quantum mechanical electron gas in adherence with Pauli's exclusion principle.

Solid plasmas are utilized for ion acceleration and have been proposed for schemes such as channeling acceleration of positively charged particles [34].
A charged particle injected along the crystallographic axis of a mono-crystalline solid can undergo a series of glancing collisions or deflections (field-mediated) with periodic row of ions in the lattice. If these interactions with individual ions are capable of trapping the charged particles within the inter-planar space, this phenomena is referred to as crystal channeling [35]. Because the basis of energy exchange process is individual interaction of charged particles with the ionic sites, this process is entirely different from plasmonics where energy is exchanged between charged particles and collective fields of Fermi electron gas oscillations.

F. PURELY ELECTROMAGNETIC VS. ELECTROSTATIC SURFACE MODES

Surface modes are critical for external excitation of modes in solid media. It is vital to mitigate sustained, direct collisions between the excitation particle or photon pulse and the ionic lattice in order to prevent complete disintegration of the beam. Direct collisional interaction between particles and the ionic lattice not only result in energy loss of beam particles by random scattering but also disrupts the beam as an entity, through a wide-range of collective instabilities. These instabilities include filamentation, hosing amongst others and can rapidly grow to completely disrupt the beam.

Large amplitude plasmonics thus utilizes surface plasmons which are excited as the beam propagates through the core region of a tube that is surrounded by conductive walls of desired free electron density.

The conventional surface plasmon (optical or microscopy beam excited) utilizes TM mode [16] which is a purely electromagnetic mode. The TM mode subtends zero focusing forces on particle beam propagating inside the channel [36]. In fact, conventional metallic cavities that form the basis of modern particle particle accelerators and light sources also utilize the TM mode sourced by radiofrequency wall currents. However, the TM mode field structure excited by a beam that is not perfectly aligned to the axis of the cavity produces large deflecting forces. Besides metallic rf cavities, experiments on excitation of the purely electromagnetic TM mode by a charged particle beam in a hollow tube of gaseous plasma have also confirmed these characteristics [37].

On the other hand, the surface crunch-in mode [13], [14], [15] being high nonlinear violates these conditions imposed by the purely electromagnetic TM mode. In contrast with the TM mode, the electrostatic surface crunch-in plasmonic mode sustains large focusing forces. These fundamental differences prevent direct comparison between the TM and surface crunch-in modes.

When the free electron Fermi gas is driven by beam fields larger than tens of MV/m, the free electron gas gains relativistic momentum. With relativistic momentum, the kinetic energy of plasmonic oscillations increases beyond the surface potential and the oscillating electron gas oscillate across the surface [6], [7]. In an enclosed geometry, the oscillating electrons that cross over from the surrounding surface into the vacuum experience a restoring force due to mutual Coulomb repulsion.

It is important to note while the electrostatic surface crunch-in mode makes it possible to access coherence limited fields per Eq.2, the particle bunches do not directly interact with the background ionic lattice. Due to this property both negatively charged as well as positively charged particles can be accelerated equally well. Apart from the injection of an electron beam, it is also possible to inject ultrashort bunches of positron [38], positive or negative muons [39].

G. ANALYTICAL MODEL OF SURFACE CRUNCH-IN PLASMON

As discussed above, large-amplitude plasmons necessitate the use of kinetic model. The kinetic model of large amplitude plasmons developed from first principles in [6] is outlined here.

Analytical equation, Eq.4 obtained from the first principles models electrons of the Fermi gas undergoing radial surface crunch-in oscillations. Here, r_t is the tube radius, n_t is the Fermi gas electron density in the tube walls, Q_b is the beam charge, r_0 is the initial equilibrium radial position of an electron, r is its instantaneous radial position, $\omega_p(n_t) = \sqrt{(4\pi e^2/m_e)\, n_t}$ (cgs units are used here) is the bulk plasmon frequency, γ_e is the relativistic factor acquired by the oscillating Fermi gas electron.

The Gaussian particle beam (excitation pulse) that excites the Fermi electron gas has a waist size σ_r and bunch length σ_z, the peak beam density is $n_{b0} = N_b/(2\pi\sqrt{2\pi}\sigma_r^2\sigma_z)$ where N_b is the number of particles in the bunch, relativistic parameters are γ_b, β_b, the instantaneous position in a longitudinal coordinate co-moving with the particle beam is $\xi = c\beta_b t - z$, $\mathcal{F}$ is the shape function of the continually focused beam and $\mathrm{sgn}[Q_b]$ is the sign of the charge.

The kinetic equation of the instantaneous position of the Fermi gas electrons constituting plasmonic oscillations underlying the surface crunch-in plasmon quoted from [6] is,

$$\frac{\partial^2 r}{\partial \xi^2} + \frac{1}{2}\frac{\omega_p^2(n_t)}{\gamma_e c^2 \beta_b^2}\,\frac{1}{r}\left[(r^2 - r_t^2)\,\mathcal{H}(r - r_t) - (r_0^2 - r_t^2)\right] + \frac{\partial^2 r}{\partial \xi^2}\bigg|_{r=r_t}\mathcal{H}(\mathrm{sgn}[Q_b](r - r_t)) = -\mathrm{sgn}[Q_b]\,\frac{\omega_p^2(n_t)}{\gamma_e c^2 \beta_b^2}\,\frac{n_{b0}(\xi)}{n_t}\int_0^r dr\,\mathcal{F}(r, z, \xi) \tag{4}$$

Existence condition of the crunch-in mode under finite wall width Δw ensures that all of the tube electrons are not "blown out" to escape the lattice ionic potential,

$$n_t \pi \left[(r_t + \Delta w)^2 - r_t^2\right] > n_{b0}\,\sigma_r^2. \tag{5}$$

To avoid trajectory crossing at the radial maxima of outward oscillating electrons r_m, all the electrons located

between r_t and r_m collectively move and bunch together to form a sheath at r_m while maintaining their initial ordering. This maximum radial displacement of outward excursion is obtained from Eq.4 for $r_t \gtrsim \sigma_r$ (distinct from flat-top beam of original work [6] where, $\sigma_r > r_t$),

$$r_m - r_t = r_t \left(\left[1 + \frac{1}{\pi} \frac{n_{b0}}{n_t} \left(\frac{\sigma_r}{r_t} \right)^2 \right]^{1/2} - 1 \right). \quad (6)$$

The net charge of electron rings in the radially inward crunch-in phase of oscillations within an infinitesimal slice thickness, dz at the longitudinal point of maximum compression $\xi = \xi_{r-min}$ using Eq.6 is,

$$\delta Q_{\max}(\xi_{r-min}) = -e\, n_t\, \pi (r_m^2 - r_t^2)\, dz. \quad (7)$$

The radial electric field due to this collective crunch-in of all the free electrons between r_m and r_t to a radius of r_t/α (where α depends upon the mode amplitude) is estimated using Gauss's law in the $r_t \gtrsim \sigma_r$ regime,

$$E_{t-r} = -\frac{2\alpha}{(2\pi)^{3/2}} \frac{eN_b}{r_t \sigma_z} = \frac{-\alpha\ 11.4\ Q_b[\mathrm{nC}]}{\sigma_z[10\mu\mathrm{m}]\mathrm{r_t}[10\mu\mathrm{m}]} \frac{\mathrm{GV}}{\mathrm{m}}. \quad (8)$$

The crunch-in wavelength is itself proportional to the tube radius r_t (evident from Fig.6). For a large tube $r_t \gg c/\omega_p(n_t)$, the crunch-in mode tends to the TM mode ($(r_m - r_t) \ll r_t$) with $\lambda_{\mathrm{crunch-in}} \to \infty$. On the other hand, for bulk solid media where $r_t \to 0$ it is $\lambda_{\mathrm{crunch-in}} \simeq 2\pi c/\omega_p(n_t)$. Therefore, semi-empirical wavelength of the surface crunch-in plasmon is,

$$\lambda_{\mathrm{crunch-in}} = \sqrt{\langle \gamma_e \rangle} \frac{2\pi c}{\omega_p(n_t)} \left[\frac{r_t}{2\pi c/\omega_p(n_t)} + 1 \right]. \quad (9)$$

The phase of relativistically corrected wavelength during which the excited free electrons crunch-in is κ, typically ≤ 0.1. The average relativistic factor of plasmonic oscillation $\langle \gamma_e \rangle = \sqrt{1 + \left(\frac{\Delta p_r}{m_e c} \right)^2}$ is estimated using the force of the beam radial fields, F_{beam} that imparts relativistic radial momentum $\frac{\Delta p_r}{m_e c} = \frac{\omega_p^2(n_t)}{c^2} \frac{1}{r_t} \left(\frac{n_{b0}}{n_t} \right) \left(\frac{\sigma_r^2 \sigma_z}{2\pi} \right)$ to the free electron Fermi gas. Using Panofsky-Wenzel theorem $\lim_{\Delta \to 0} E_{t-r}/\Delta\xi = E_{t-z}/(2\pi\, \Delta r)$ [40] where $\Delta r = r_m - r_t$ and $\Delta\xi = \kappa\, \lambda_{\mathrm{crunch-in}}$, the maximum longitudinal electric field E_{t-z} is estimated under $r_t \gtrsim \sigma_r$,

$$\begin{aligned} E_{t-z} &= \frac{-2e\, \alpha \kappa^{-1}}{(2\pi)^{1/4}} \frac{\sqrt{N_b n_t r_t}}{\sigma_z} \frac{\sqrt{1 + \frac{1}{\pi} \left(\frac{n_{b0}}{n_t} \right) \frac{\sigma_r^2}{r_t^2}} - 1}{1 + r_t/\lambda_p} \\ &= -5.2\, \frac{\alpha}{\kappa} \frac{\sqrt{Q_b[\mathrm{nC}]\, n_t[10^{18}\mathrm{cm}^{-3}]\, r_t[10\mu\mathrm{m}]}}{\sigma_z[10\mu\mathrm{m}]} \\ &\quad \times \frac{\sqrt{1 + \frac{1}{\pi} \left(\frac{n_{b0}}{n_t} \right) \frac{\sigma_r^2[10\mu\mathrm{m}]}{r_t^2[10\mu\mathrm{m}]}} - 1}{1 + r_t/\lambda_p} \frac{\mathrm{GV}}{\mathrm{m}}. \end{aligned} \quad (10)$$

H. DYNAMIC APERTURE INTERPRETATION OF ELECTROSTATIC SURFACE MODES

From the Panofsky-Wentzel theorem [40] applied to purely electromagnetic surface modes such as the TM mode at a given frequency it follows that when the longitudinal field of a charge located inside a structure increases with miniaturization as $1/a^2$, where a is the "fixed" transverse dimension of a tube (r_t at equilibrium), the transverse field amplitude increases as $1/a^3$.

These purely electromagnetic transverse fields are unfavorable and lead to head-tail and beam breakup (BBU) instabilities that severely limit the amount of charge that can be accelerated in miniaturized devices. Moreover, transverse misalignment between the beam axis and the axis of symmetry of the structure excites higher-order modes that deflect the beam off-axis.

On the other hand, this scaling can be overcome with "dynamic" transverse aperture, $a(\xi)$ as is the case in electrostatic surface crunch-in mode. The head of an electron beam drives the free electrons Fermi gas outwards which as part of its oscillation trajectory goes across the surface and re-converges on the axis behind the driver. The aperture behind the beams $a(\xi_{\min})$, can be vanishingly small and result in large accelerating fields, while the aperture seen by the head of the beam ($r_t \gtrsim \sigma_r$) and associated with the transverse fields is much larger. The dynamic aperture of electrostatic modes can overcome the scaling limitations that otherwise limit purely EM modes.

IV. LARGE-AMPLITUDE SEMICONDUCTOR PLASMONICS: COMPUTATIONAL MODEL

A. KINETIC MODELING OF LARGE-AMPLITUDE PLASMONICS AND SIMULATION SETUP

The relativistic and nonlinear plasmonic modes excited in conductive materials need to solve the full set of Maxwell's equation unlike the free-space (zero charge and current densities, $\rho_e = J_e = 0$) assumption behind purely electromagnetic solver. Nonlinear plasmons that are strongly electrostatic do not lend themselves to being modeled using purely electromagnetic codes.

Conventional optical plasmons are typically modeled using Finite-Difference-Time-Domain (FDTD) method where the perturbative electron oscillations are simply approximated using constitutive parameters. The FDTD approach cannot be used when the trajectories of collective electron oscillations attain amplitudes which are a significant fraction of plasmonic wavelength resulting in large-scale charge density displacement. Large density displacement leads to highly localized, rapid spatial variation of material properties such as permittivity which necessitate a non-perturbative approach.

Our work has adopted the kinetic approach along with particle-tracking Particle-In-Cell (PIC) computational modeling of collective oscillations of the free electrons Fermi gas to account for the nonlinear characteristics of strongly electrostatic plasmons. Specifically, the PIC methodology incorporates charge and current densities by tracking representative particles within the FDTD solver to calculate the net electromagnetic fields. In addition, it also calculates the effect of the updated fields on the charge and current densities and accordingly pushes particles under the action

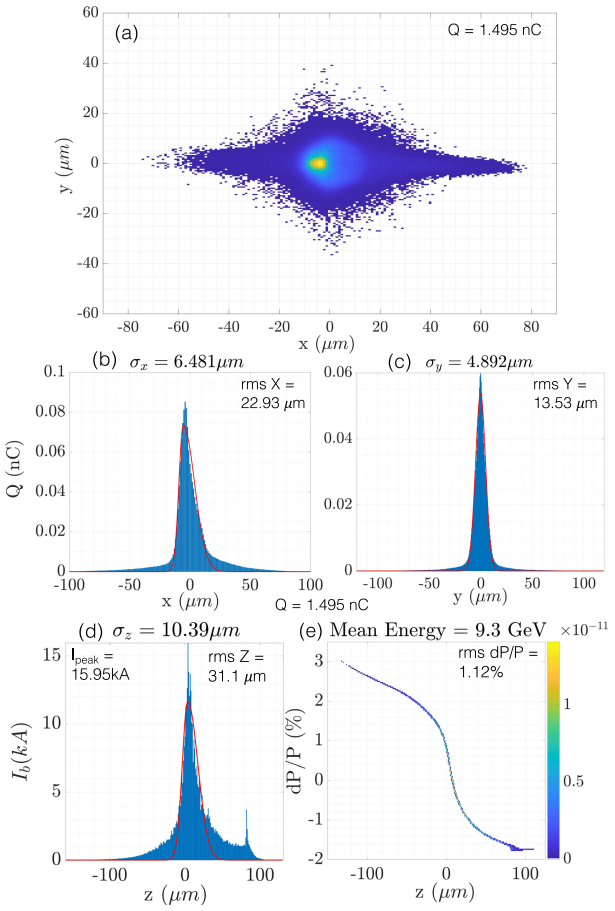

FIGURE 5. Simulated phase-space slices of early stage FACET-II electron beam: (a) beam transverse profile, (b,c) transverse spatial distribution, (d) longitudinal spatial distribution, (e) longitudinal momentum phase-space. Estimated standard deviation (σ) and root-mean-square (rms) of the spatial distribution are obtained from a Gaussian fit.

of the net EM fields obtained using FDTD completing the loop. This approach is based upon collisionless nature of relativistic oscillations of the Fermi gas which stems from relativistically induced ballistic electron transport explained in sec.III-D. In this methodology, no constitutive parameters are initialized to model materials. Nonetheless, initialization and self-consistent evolution of electron charge and current densities implicitly accounts for effects that the constitutive parameters represent in an averaged sense.

However, as relativistic oscillations of the free electron Fermi gas have been experimentally observed to go beyond Ohm's law, the long-term evolution of these oscillations and the effect on ionic lattice requires further development. Specifically, conductivity which is a critical constitutive parameter based upon average electron-ion collisions needs further experimental investigations to be properly understood in the relativistic plasmonic regime.

The 3D PIC simulation in Fig.1 that models the semiconductor surface crunch-in plasmon is setup over a cartesian spatial grid of $160 \times 80 \times 80\mu m^3$ resolved with 200nm cubic cells. The free electron Fermi gas density of $n_t = 10^{18}\text{cm}^{-3}$ in the n-type doped semiconductor tube of square cross-section is modeled using 4 particles per cubic cell with fixed ions. The length of a side of the square cross-section is, $r_t = 12.5\mu$m and wall thickness $\Delta w = 25\mu$m. Realistic electron beam profile to enable experimental verification (described in sec.IV-B) with peak density $n_{b0} = 10^{18}\text{cm}^{-3}$; waist-size $\sigma_r \simeq 5\mu$m ($r_t = 2.5 \times \sigma_r$) and bunch length $\sigma_z \simeq 10\mu$m is initialized with 2 particles per cell. The box copropagates with the ultrarelativistic beam that has a relativistic factor $\gamma_b \simeq 2 \times 10^4$. Absorbing boundary conditions are used for both fields and particles.

The parameters of the crunch-in mode observed from 3D PIC simulation in a tube with square cross-section are in good agreement with our kinetic model (of sec.III-G) in cylindrical symmetry. The crunch-in wavelength $\lambda_{\text{crunch-in}}$ per Eq.9, $\langle\gamma_e\rangle \times 45\mu$m agrees well with the 50μm observed in Fig.2. Eq.8 (Eq.10) predicts a peak focusing field (accelerating field) of around $E_{t-r} \simeq 13.7\alpha$ GV/m ($E_{t-z} \simeq 9.3\alpha$ GV/m with $\kappa = 0.1$) which agrees well with Fig.2, top panel $E_{t-r} \simeq 20$ GV/m (Fig.2, bottom panel $E_{t-z} \simeq 15$ GV/m).

The 2.5D PIC (2 spatial and 3 velocity dimensions) simulation in sec.IV-C, IV-D and IV-E utilize cartesian spatial grid with 100nm square cells. The particles of free electron Fermi gas are modeled with 9 macro-particles per cell and the particles of the beam with 4 macro-particles per cell. Beam profile is initialized as per simulated transverse and longitudinal beam phase-spaces in sec.IV-B.

B. PHASE-SPACE OF A READILY ACCESSIBLE TEN MICRON, NANO-COULOMB ELECTRON BEAM

Our kinetic simulations utilize parameters of currently available beam at FACET-II facility directly from a beam dynamics simulation. This start-to-end beam dynamics simulation incorporates the FACET-II electron injector, linac and compression systems. The injector comprises a high-gradient copper cathode rf gun, 125 MeV s-band linac and double-bend system to inject into the main s-band linac. The emittance of the 2nC bunch injected from the gun is 5 mm-mrad. This section of beamline is modeled using the General Particle Tracer (GPT) tracking code [41], which accounts for 3D space charge as well as rf cavity wakefields in the s-band structures.

Particles from GPT simulation are passed to the Lucretia code [42] which models the rest of the beamline. This includes three additional s-band acceleration sections and three stages of bunch compression at 335 MeV, 4.5 GeV and 10 GeV. Longitudinal and transverse wakefields are modeled in the s-band rf structures. Incoherent (ISR) and coherent (CSR) synchrotron radiation effects [43] are modeled in the compression chicane bends while longitudinal space charge effect is modeled through the entire accelerator chain.

From simulations, at a minimum final beta function (distance over which focussed beam diverges to two times the area at its focal waist) of 5 cm (at 10 GeV), the minimum

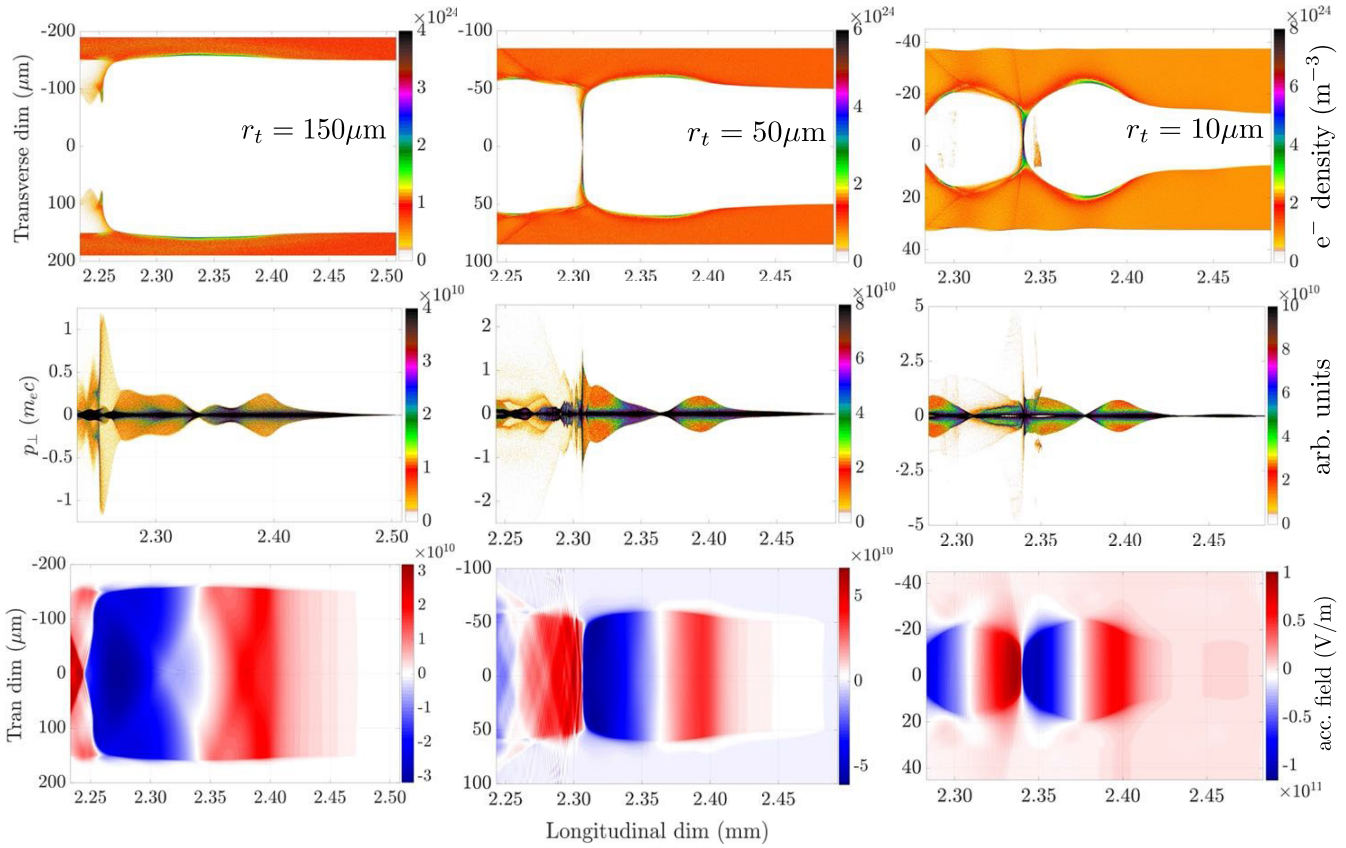

FIGURE 6. Semiconductor surface crunch-in plasmonic mode excited in tubes of different radius r_t = 150, 50, 10μm after 2.4mm of interaction. Top row shows the free electron density profile in m^{-3}, middle row the transverse momentum vs. longitudinal spatial dimension phase-space (in arbitrary units) and bottom row the longitudinal electric field in V/m.

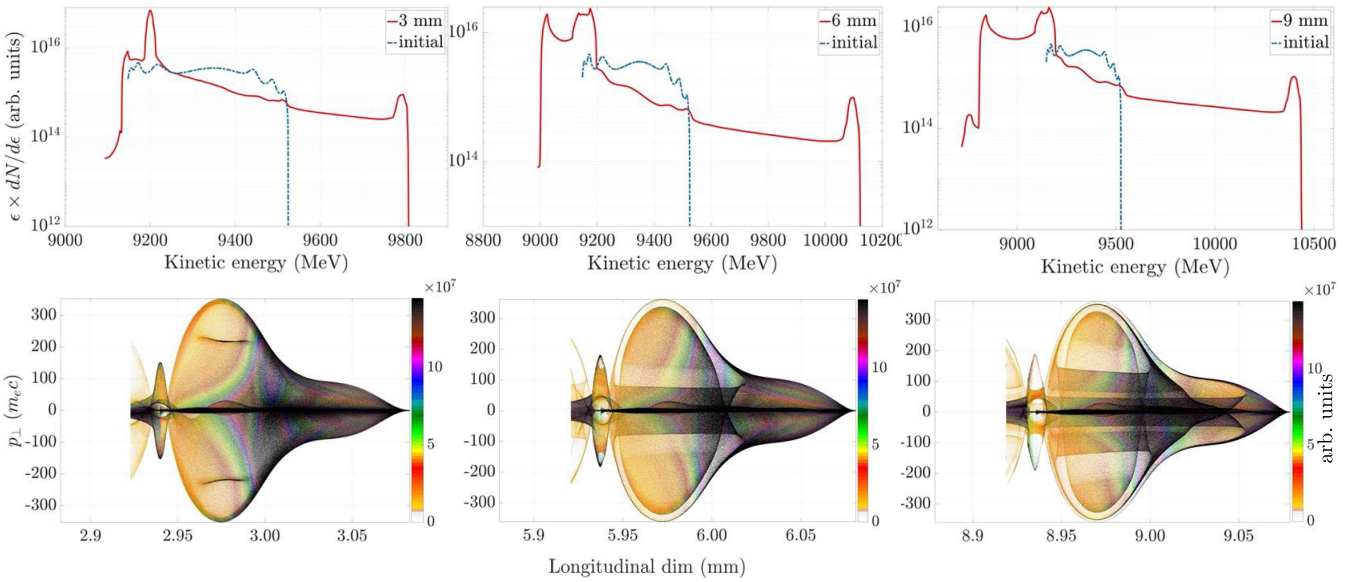

FIGURE 7. Length scan over 3,6 and 9 mm (left to right column respectively) of beam interaction with plasmonic fields which results in experimentally measurable changes in the beam energy spectra (top row) and transverse phase-space (transverse momentum vs. longitudinal spatial dimension) of the electron beam (bottom row) for $r_t = 20\mu$m.

vertical beam waist-size is found to be about 4μm, and the horizontal spot size depends on the final bunch length (due to CSR emittance degradation in the final bunch compressor). Fig.5 shows particle distributions for transverse and longitudinal phase space slices of early stage FACET-II electron beam.

C. SCALING OF SURFACE CRUNCH-IN PLASMON WITH TUBE DIMENSIONS

A scan over the radius of semiconductor tube, r_t at fixed free electron Fermi gas wall density $n_t = 10^{18}\text{cm}^{-3}$ using 2.5D PIC simulations (cartesian grid) is summarized in Fig.6. It demonstrates matched excitation of semiconductor surface crunch-in plasmon is robust and its properties such as wavelength, Eq.9 can be further tuned by choosing appropriate tube radius. Corresponding variation of the oscillation momentum of the Fermi gas (middle row of Fig.6) and longitudinal field strengths (bottom row of Fig.6) are compared for $r_t = 150, 50, 10\mu$m.

Firstly, over this range of tube radii the crunch-in mode is consistently excited as the electron gas gains relativistic momentum ($\langle\gamma_e\rangle \gg 1$) and almost instantaneously tunnels through the surface. The mutual electrostatic repulsive force of free electrons that collectively tunnel and accumulate inside the tube provides restoring force which sets up the oscillations. Unlike [6], here the tube encloses nearly the entire beam in the transverse direction with $r_t > \sigma_r$, except for a small fraction in the wings of the beam that directly interacts with the lattice.

Secondly, radial scan helps verify the kinetic model of plasmon in Eq.4 and the parameters derived from it. With decreasing tube radius r_t, an increase in maximum radial displacement of electron gas $\Delta r = r_m - r_t$ per Eq.6, crunch-in wavelength per Eq.9 and the field strength per Eq.10 is observed (in proportion with increasing radial momentum gain of electron gas).

Similar to 3D PIC simulations, a good agreement is observed between simulations and analytical expressions for various derived quantities. The variation in longitudinal and focusing fields observed for varying tube radius is found to be significant enough to be discernible in experiment as described in sec.IV-D. The first stage of material fabrication makes it possible to study these effects in square semiconductor tubes with 30 and 100μm sides.

Importantly, although the beam as modeled in sec.IV-B is initially misaligned relative to the tube axis with the beam centroid offset in the negative x-direction as seen in Fig.5(a), there is no observation of the onset of filamentation or hosing instability in the 3D and 2.5D simulations. This suppression of instabilities is observed over centimeter scale interaction lengths nearly equal to the beam beta function of about 5cm.

Relativistic momentum gain of the free electron Fermi gas is observed over the range of radii modeled in the simulations. Therefore, relativistically induced ballistic transport dominates and Ohm's law cannot be applied.

However, the magnitude of relativistic momentum decreases with increasing tube radius and further investigations are required to determine the threshold of transition from ballistic to Ohmic transport.

D. OBSERVABLE EFFECTS OF PLASMONIC FIELDS

Experimentally observable effects of plasmonic fields on the beam are modeled using 2.5D PIC (cartesian grid) simulations. The tube length is varied over a range of the ongoing structured semiconductor fabrication effort (described in sec.V) with a fixed tube radius $r_t = 20\mu$m.

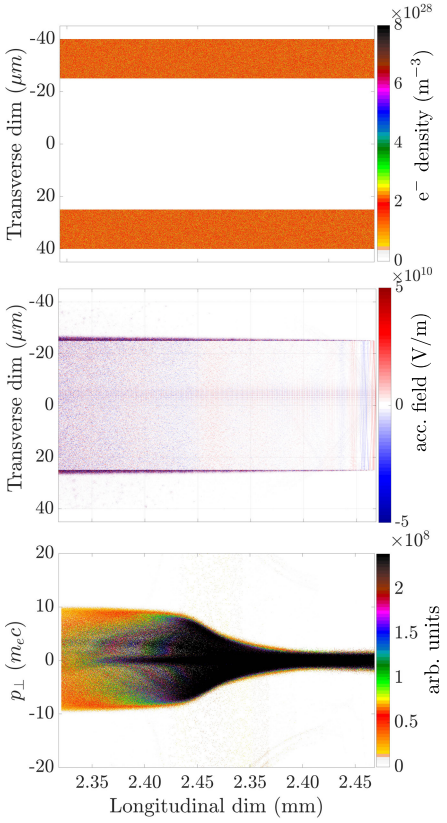

FIGURE 8. Electron density profile (top), accelerating field (middle) and beam transverse momentum phase-space (bottom) after 8ps of interaction between a metallic tube with free electron density, $n_t = 2 \times 10^{22}\text{cm}^{-3}$ excited by the nC, ten micron beam described in sec.IV-B.

Focusing and acceleration of electron beam under the action of the fields of crunch-in plasmon is summarized in Fig.7 using a length scan over 3, 6 and 9 mm long semiconductor tube (left to right columns, respectively).

Fig.7 (top row) demonstrates the acceleration of a significant fraction of the beam particles by many hundreds of MeV over sub-centimeter tube lengths. Specifically, nearly a GeV energy gain with a quasi-monoenergetic peak at around 10.4GeV (compared to the initial mean beam energy of 9.3GeV observed from Fig.IV-B(e)) is observed over 9 mm of interaction length. This energy gain in significantly higher than the initial energy spread of the beam evident in Fig.IV-B(e).

The average accelerating field of about 100GV/m evident in Fig.6 for $r_t = 10\mu m$ is in very good agreement with eq.10. Note that over longer interaction lengths the particles in the beam wings get focussed into the tube (beam self-focusing effect) which increases the beam fields at $r \geq r_t$ and as a result the plasmonic fields.

The action of the focusing fields of the surface crunch-in plasmon is experimentally quantifiable based upon the

modification of the transverse momentum phase-space of the beam along the longitudinal dimension in the bottom row of Fig.7. The changes in this phase-space imprint themselves on spatial modulation of the beam envelope observed downstream from the interaction region (after the dispersion dipole magnet). The opening angle observed is around 16 milli-radians ($p_\perp/p_\parallel = 320/19800 \simeq 16 \times 10^{-3}$rad). Moreover, the transverse phase-space has a specific structure due to the structure of the plasmonic focusing fields.

The aforementioned effects of the acceleration and focusing of an electron beam under plasmonic fields can be resolved using existing beam diagnostics. These results are exactly applicable to other beams that have a larger waist-sizes but are enclosed within the tube radius. Moreover, these results model the underlying physics and are not intended to be specific to any beam.

E. SEMICONDUCTOR VS. METALLIC, DIELECTRIC TUBE

A critical aspect of plasmonic modes is the ability to tune the conduction band electron density and thereby control the free electron Fermi gas density which makes it possible to match with readily available beams. Here a comparison of plasmon excitation in tubes with walls of semiconductor versus metal (modeled in [6]) using currently available nC, ten micron electron beam described in sec.IV-B is used to demonstrate this. While semiconductor material with free electron density of 10^{18}cm^{-3} has a characteristic plasmon size of 33μm, for metallic free electron density of 2×10^{22}cm^{-3} it is only 250nm. The currently accessible beam dimensions of $\sigma_r, \sigma_z \simeq 10\mu$m and the peak beam density $n_{b0} \simeq 10^{18}$cm^{-3} are therefore largely mismatched with that of metallic plasmons modeled in [6].

Simulation of plasmonic mode excited by the nC, ten micron electron beam is summarized in Fig.8. The excited free electron density profile (top), acceleration field (middle) and beam transverse phase-space (bottom) is presented after 8ps of interaction.

It is evident that the profile of the acceleration field in metallic density excited under the heavily mismatched condition hardly has any spatial structure or features. Consequently, no net acceleration or deceleration of beam particles is observed unlike for a semiconductor plasmon in the middle row of Fig.6. Similarly, on average the focusing fields have an almost negligible effect on the beam. From the almost featureless beam transverse phase, the maximum opening angle of beam particles under the action of metal plasmons is only 5×10^{-4} rad while in comparison it is 15.2 milli-rad (experimentally discernble) for the semiconductor plasmons as seen in bottom row of Fig.7 along with an imprint of plasmonic focusing fields.

On the other hand, a dielectric tube of similar dimension made of silica (SiO_2, an insulator) but without a metallic coating is used for direct comparison with plasmons. Per the discussion in sec.III-E.a, an uncoated dielectric tube does not trap the Cherenkov radiation and therefore no observable effects on the beam except the few MeV energy lost to radiation, are expected.

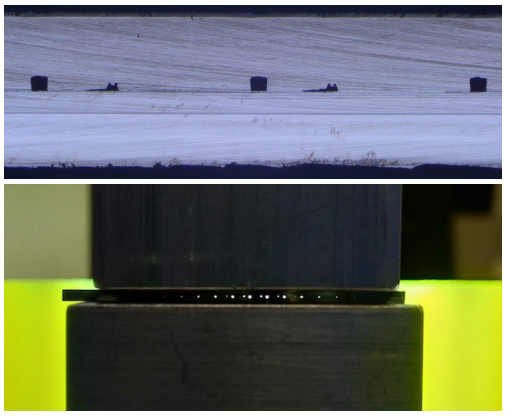

FIGURE 9. SEM based cross-section of semiconductor tubes (top) with $100 \times 100\mu$m^2 and $30 \times 30\mu$m^2 core regions stacked adjacent to each other in a 3mm end-to-end zoomed-in field-of-view. Light passing through the length of these tubes (bottom).

V. STRUCTURED SEMICONDUCTOR FABRICATION

The first stage of semiconductor plasmonic structures have been fabricated on Silicon wafers of 100mm diameter polished on a single side. These wafers were 525μm thick with $\langle 100 \rangle$ orientation and chosen with either high resistivity (20Ω-cm) or low resistivity (0.025Ω-cm). The n-type doped low resistivity wafer corresponds to a conduction band free electron density of about 10^{18}cm^{-3}. The wafers were cleaned using standard procedures, coated with AZ P4330 photoresist and groups of channels 30 and 100 μm wide, approximately 1.5mm apart and a range of lengths 3-30mm, were defined using a direct write laser exposure (maskless) lithography. Deep reactive ion etching (DRIE) was used to etch channels of square cross section. A second wafer was processed similarly except that the etching was done on the rough, unpolished side of the wafer. The polished sides of the two wafers were put in contact in an evacuated chamber and then transferred to an oven where they were annealed at 1100°C in Nitrogen atmosphere for three hours to form a permanent bond. The etched pattern in the top unpolished surface served as a guide to saw the wafer into pieces with groups of channels of the same length.

The top panel of Fig.9 is 3mm wide expanded view of the prepared semiconductor sample showing three 100μm and two 30μm channels. The bottom panel is a full end-to-end view of the structure showing light passing through the adjacent pairs of 100μm and 30μm square channels of 3mm length. Relative ease of first aligning the beam with wider channels makes it possible to experimentally converge towards smaller channels that are at a fixed distance from the already aligned wider ones.

VI. TOWARDS MEGA-AMPERE CURRENTS: SUB-MICRON BEAMS

While structured semiconductors are used to match with currently accessible ten micron bunches, the ultimate reach

of PV/m plasmonics is attainable in materials with highest free electron densities. However, matched excitation of such metallic plasmons requires sub-micron bunch lengths and waist-sizes which closely align with ongoing trends in bunch compression. This section summarizes ongoing efforts and challenges behind MegaAmpere (MA) peak currents using submicron, nC bunches.

A. SUB-MICRON BUNCH LENGTH COMPRESSION OF nC CHARGE BEAMS

Recent advances in beam phase-space rotation based bunch length compression techniques [44] has opened up the possibility of sub-micron bunch lengths with multi-MA peak currents. Matched excitation of plasmons in metals relies on compression of bunch length and focusing of bunch waist to sub-micron dimensions.

Ongoing upgrades at the FACET-II facility of the Stanford Linear Accelerator Center (SLAC) are expected to provide greater than 200kA pulses with less than 1μm rms bunch length in the near future. The precedent to sub-micron bunches was set by 20 to 30μm rms bunch length, with 30kA peak current that were in operation at the same facility during the last decade.

Extension of longitudinal compression of electron bunches into the 100 nm, multi-MA regime has been modeled in recent feasibility studies [11].

The regime of multi-MA peak current compression requires next-generation high-brightness electron injector apart from mitigation of various non-linearities present in the compression process to preserve both longitudinal and transverse properties of the bunch such as emittance.

Extreme compression is limited primarily by coherent synchrotron radiation (CSR) [43] in various bends which causes transverse emittance growth of many orders of magnitude, in addition to greatly limiting the final achievable peak current. To compensate for emittance degradation due to CSR, more complex compression chicane designs beyond the standard 4-bend chicane have been considered, e.g. multi-bend chicanes, quadrupole and sextupole loaded chicanes, arcs or wigglers.

The key design parameters, constraints and considerations for a bunch compressor capable of compression of electron bunch to peak currents $>$ 0.3 MA (1nC bunch compressed to 1μm bunch length) with $<$ 1mm $-$ mrad transverse emittance growth are:

1) an advanced photo-injector with transverse emittance $<$ 1mm $-$ mrad, 1-2 nC charge, few 100A initial peak current ($\sim$ 3mm initial bunch length at the injector) and typical injector energy of $\sim$ 100MeV.
2) initial injector charge $>$ 2nC to allow for collimation of tails or wings formed during compression.
3) multi-stage compression to achieve bunch length compression ratios of $>$ 1000 as stage-wise compression removes the need for excessive energy spread to achieve such large compression ratios. For example, FACET-II uses three compression stages at 0.3, 4.5, 10 GeV beam energy along the linear accelerator.
4) final compression needs to be at the final beam energy to account for the following effects:
   - relative emittance growth due to CSR decreases with beam energy as $\Delta\epsilon_n/\epsilon_n \sim 1/\sqrt{\gamma}$
   - adverse surface effects in accelerator components are expected at the highest compression (ohmic pulse heating) and the final compression stage minimizes the interaction at maximum compression
   - energy chirp induced by cavity wakefields in the final accelerating section is utilized. The final compression stage should have positive longitudinal momentum to space correlation parameter $R_{56} > 0$, with higher energy particles at the head of the bunch, to utilize cavity wakefield chirp. This also helps with non-linearities from compression system (T_{566}) with partial self-cancelation from rf curvature.

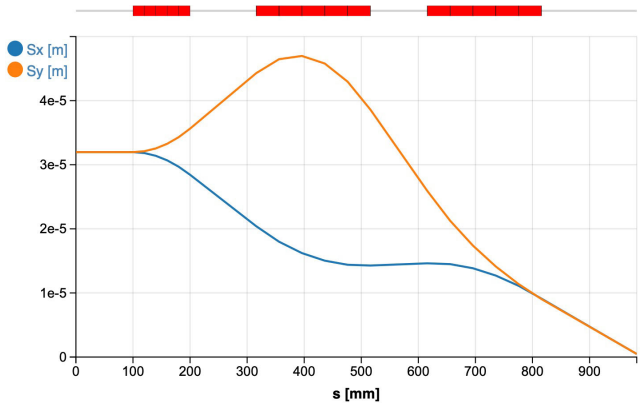

FIGURE 10. Particle-tracking simulation [47] demonstrating the compression of an electron beam initially with ten micron waist-size $\sigma_{x,y} \sim 10\mu$m to $<$ 500nm in a 1 m-long PMQ by first defocusing it to about 30μm coming into the PMQ.

Initial compression stages reduce the bunch length to 20μm rms, where the peak current is a 12 kA, similar to the largest values used at FEL facilities, where emittance preservation has been experimentally demonstrated at low charge ($<$ 200 pC).

To achieve the desired positive R_{56} compression for the final compression stage a quadrupole-loaded lattice such as an arc or wiggler (depending on whether net-bending is a desired feature or not) is required.

A proof-of-principle model using the tracking code Lucretia [42] utilized a wiggler system for the tasks of the final compressor. This design uses a triplet-based arc wiggler (9 cells) with a total bend angle of 67 mrad at 30 GeV. This provides $+$17mm of R_{56} in a length of 150m whilst keeping emittance growth to $<$ 5% due to incoherent synchrotron radiation in the bends. Sextupoles are included in the optics to provide cancelation of CSR energy kicks. The maximum compression for this design is limited at 375 kA,

with 5 mm-mrad of slice emittance growth. Further work is ongoing to control emittance growth and achieve higher peak currents.

B. SUB-MICRON WAIST-SIZE COMPRESSION WITH PERMANENT MAGNET QUADRUPOLES (PMQs)

In order to attain beam waist-size optimal for matched excitation of the crunch-in mode in materials with metallic density, an appropriate focusing scheme is required. Furthermore, in realistic experimental scenarios where interaction regions are constrained in space, the focusing system should be compact and robust. A magnetic focusing system that can work along with plasmonic nanofocusing [10] is modeled.

PMQs are ideal focusing elements for small spot size applications as they are able to provide very high magnetic field gradients. These gradients can be in excess of 700 T/m [45] for rare-earth magnets and up to 3000T/m in nanofabricated designs [46] in a compact form factor. However, quadrupoles only provide focusing in one dimension, while defocusing the beam in the other. Hence, the simplest configuration of permanent magnet quadrupoles for overall focusing requires a triplet configuration. The triplet system is tunable by the relative reconfiguration of quadrupole locations. Hybrid configurations, with steel, can be used to incorporate split designs for limited access.

For the present configuration, consideration of the limited space upstream of the structure is critical such that both high intensity, and adequate interaction length is achievable. So, only configurations constrained to < 1m are considered. In order to attain this goal, permanent magnet quadrupoles with gradient ~ 750T/m are used in a triplet layout shown as red blocks in Fig.10, with lengths of 10cm, 20cm, and 20cm respectively. The final spot size using this triplet is just below 500nm in both the transverse dimensions. A defocusing arrangement downstream of the focal locations with mirror symmetry would transport the spent beam.

VII. CONCLUSION

The tunability of Fermi electron gas in structured semiconductors allows matched excitation of large-amplitude surface plasmons using a range of currently accessible electron beams. It is computationally demonstrated that by using n-typed doped semiconductors with free electron Fermi gas density of about 10^{18}cm^{-3} the plasmonic mode dimensions match currently available ten micron, nC electron beam.

Tunable plasmons, therefore, make it possible to undertake immediate experimental verification of the principles underlying Petavolts per meter plasmonics, including relativistic ballistic transport and relativistic tunneling of oscillating electrons across the surface. Excitation of large-amplitude, surface crunch-in plasmonic mode in semiconductor tubes is modeled to sustain tens of GV/m acceleration and focusing fields inside the tube. Such large plasmonic fields not only accelerate a significant number of beam particles resulting in hundreds of MeV energy gain in sub-centimeter long tubes but also focus the beam resulting in tens of milli-radian angular deviation. In contrast, metallic and dielectric tubes of similar dimensions do not produce these effects.

Experimental validation of the underlying details of Petavolts per meter plasmonics using tunable semiconductor structures hand in hand with the ongoing MegaAmpere sub-micron beam effort can open transformative pathways in fundamental science and technological applications greatly enhancing the frontiers of electromagnetism.

REFERENCES

[1] D. Bohm and D. Pines, "A collective description of electron interactions: III. Coulomb interactions in a degenerate electron gas," *Phys. Rev.*, vol. 92, no. 3, pp. 609–625, Nov. 1953, doi: https://doi.org/10.1103/PhysRev.92.609.

[2] R. H. Ritchie, "Plasma losses by fast electrons in thin films," *Phys. Rev.*, vol. 106, no. 5, pp. 874–881, Jun. 1957, doi: 10.1103/PhysRev.106.874.

[3] F. Bloch, "Über die quantenmechanik der elektronen in kristallgittern," *Zeitschrift für Physik*, vol. 52, nos. 7–8, pp. 555–600, Jul. 1929, doi: 10.1007/BF01339455.

[4] S. A. Maier, M. L. Brongersma, P. G. Kik, S. Meltzer, A. A. G. Requicha, and H. A. Atwater, "Plasmonics: A route to nanoscale optical devices," *Adv. Mater.*, vol. 13, no. 19, pp. 1501–1505, 2001, doi: 10.1002/1521-4095(200110)13:19<1501::AID-ADMA1501>3.0.CO;2-Z.

[5] F. J. García de Abajo, "Optical excitations in electron microscopy," *Rev. Modern Phys.*, vol. 82, no. 1, pp. 209–275, Feb. 2010, doi: 10.1103/RevModPhys.82.209.

[6] A. A. Sahai, "Nanomaterials based nanoplasmonic accelerators and light-sources driven by particle-beams," *IEEE Access*, vol. 9, pp. 54831–54839, 2021, doi: 10.1109/ACCESS.2021.3070798.

[7] A. A. Sahai, "Emergence of TeraVolts per meter plasmonics using relativistic surface plasmonic modes," *Proc. SPIE*, vol. 11797, Aug. 2021, Art. no. 117972A, doi: 10.1117/12.2596637.

[8] A. A. Sahai, "Nanostructure nanoplasmonic accelerator, high-energy photon source, and related methods," WO Patent 2021216424 A1, Oct. 28, 2021. [Online]. Available: https://patentimages.storage.googleapis.com/55/0a/6c/7b757efb9e9547/WO2021216424A1.pdf

[9] J. M. Dawson, "Nonlinear electron oscillations in a cold plasma," *Phys. Rev.*, vol. 113, no. 2, pp. 383–387, Jan. 1959, doi: 10.1103/PhysRev.113.383.

[10] A. A. Sahai, "Plasmonic nano-focusing of particle beams by surface crunch-in plasmons excited in tapered tubes," *Proc. SPIE*, vol. 11999, Mar. 2022, Art. no. 1199903, doi: 10.1117/12.2605722.

[11] G. White, "FACET-II start-to-end simulations of electron beam," in *Proc. FACETII Sci. Workshop*, 2019, pp. 2–17. [Online]. Available: https://www.slac.stanford.edu/~whitegr/F2_S2E/F2_S2E.pdf

[12] *Conceptual Design Report for the FACET-II Project, Section 3.3.1*, Office High Energy Physics, U.S. Dept. Energy, Washington, DC, USA, SLAC-R-1067, Apr. 2016. [Online]. Available: https://slac.stanford.edu/pubs/slacreports/reports21/slac-r-1067.pdf

[13] A. A. Sahai, "Excitation of a nonlinear plasma ion wake by intense energy sources with applications to the crunch-in regime," *Phys. Rev. Accel. Beams*, vol. 20, no. 8, Aug. 2017, Art. no. 081004, doi: 10.1103/PhysRevAccelBeams.20.081004.

[14] A. A. Sahai, "On certain non-linear and relativistic effects in plasma-based particle acceleration," M.S. thesis, Dept. Elect. Eng., Duke Univ., Durham, NC, USA, 2015. [Online]. Available: https://dukespace.lib.duke.edu/dspace/handle/10161/10534

[15] A. A. Sahai and T. C. Katsouleas, "Optimal positron-beam excited wake-fields in hollow and ion-wake channels," in *Proc. Int. Particle Accelerator Conf.*, Richmond, VA, USA, 2015, pp. 2674–2677, doi: 10.18429/JACoW-IPAC2015-WEPJE001.

[16] T. K. Sarkar, M. N. Abdallah, M. Salazar-Palma, and W. M. Dyab, "Surface plasmons-polaritons, surface waves, and Zenneck waves: Clarification of the terms and a description of the concepts and their evolution," *IEEE Ant. Prop. Mag.*, vol. 59, no. 3, pp. 77–93, May 2017, doi: 10.1109/MAP.2017.2686079.

[17] A. P. Roth, J. B. Webb, and D. F. Williams, "Band-gap narrowing in heavily defect-doped ZnO," *Phys. Rev. B, Condens. Matter*, vol. 25, no. 12, pp. 7836–7839, Jun. 1982, doi: 10.1103/PhysRevB.25.7836.

[18] A. Agrawal, S. H. Cho, O. Zandi, S. Ghosh, R. W. Johns, and D. J. Milliron, "Localized surface plasmon resonance in semiconductor nanocrystals," *Chem. Rev.*, vol. 118, no. 6, pp. 3121–3207, Mar. 2018, doi: 10.1021/acs.chemrev.7b00613.
[19] S. J. Gamble, M. H. Burkhardt, A. Kashuba, R. Allenspach, S. S. P. Parkin, H. C. Siegmann, and J. Stöhr, "Electric field induced magnetic anisotropy in a ferromagnet," *Phys. Rev. Lett.*, vol. 102, no. 21, May 2009, Art. no. 217201, doi: 10.1103/PhysRevLett.102.217201.
[20] J. Towns, T. Cockerill, M. Dahan, I. Foster, K. Gaither, A. Grimshaw, V. Hazlewood, S. Lathrop, D. Lifka, G. D. Peterson, R. Roskies, J. R. Scott, and N. Wilkins-Diehr, "XSEDE: Accelerating scientific discovery," *Comput. Sci. Eng.*, vol. 16, no. 5, pp. 62–74, Sep. 2014, doi: 10.1109/MCSE.2014.80.
[21] J. Anderson, P. J. Burns, D. Milroy, P. Ruprecht, T. Hauser, and H. J. Siegel, "Deploying RMACC summit: An HPC resource for the rocky mountain region," in *Proc. Pract. Exper. Adv. Res. Comput. Sustainability, Success Impact*, Jul. 2017, pp. 1–7, doi: 10.1145/3093338.3093379.
[22] T. D. Arber, K. Bennett, C. S. Brady, A. Lawrence-Douglas, M. G. Ramsay, N. J. Sircombe, P. Gillies, R. G. Evans, H. Schmitz, A. R. Bell, and C. P. Ridgers, "Contemporary particle-in-cell approach to laser-plasma modelling," *Plasma Phys. Controlled Fusion*, vol. 57, no. 11, Nov. 2015, Art. no. 113001, doi: 10.1088/0741-3335/57/11/113001.
[23] J. Schwinger, "On gauge invariance and vacuum polarization," *Phys. Rev.*, vol. 82, no. 5, pp. 664–679, Jun. 1951, doi: 10.1103/PhysRev.82.664.
[24] M. I. Stockman, "Nanofocusing of optical energy in tapered plasmonic waveguides," *Phys. Rev. Lett.*, vol. 93, no. 13, Sep. 2004, Art. no. 137404, doi: 10.1103/PhysRevLett.93.137404.
[25] G. Amelino-Camelia, J. Ellis, N. E. Mavromatos, and D. V. Nanopoulos, "Distance measurement and wave dispersion in a Liouville-string approach to quantum gravity," *Intl. J. Modern Phys. A*, vol. 12, no. 3, pp. 607–623, 1997, doi: 10.1142/S0217751X97000566.
[26] I. Tudosa, C. Stamm, A. B. Kashuba, F. King, H. C. Siegmann, J. Stöhr, G. Ju, B. Lu, and D. Weller, "The ultimate speed of magnetic switching in granular recording media," *Nature*, vol. 428, no. 6985, pp. 831–833, Apr. 2004, doi: 10.1038/nature02438.
[27] W. Pauli, "The connection between spin and statistics," *Phys. Rev.*, vol. 58, no. 8, pp. 716–722, Oct. 1940, doi: 10.1103/PhysRev.58.716.
[28] C. F. V. Weizsacker, "Ausstrahlung bei Stossen sehr schneller elektronen," *Zeitschrift für Physik*, vol. 88, nos. 9–10, pp. 612–625, Sep. 1934, doi: 10.1007/BF01333110.
[29] E. J. Williams, "Nature of the high energy particles of penetrating radiation and status of ionization and radiation formulae," *Phys. Rev.*, vol. 45, no. 10, pp. 729–730, May 1934, doi: 10.1103/PhysRev.45.729.
[30] M. S. Shur and L. F. Eastman, "Ballistic transport in semiconductor at low temperatures for low-power high-speed logic," *IEEE Trans. Electron Devices*, vol. ED-26, no. 11, pp. 1677–1683, Nov. 1979, doi: 10.1109/T-ED.1979.19671.
[31] R. H. Fowler and L. W. Nordheim, "Electron emission in intense electric fields," *Proc. Roy. Soc. London A, Containing Papers Math. Phys. Character* vol. 119, pp. 173–181, May 1928, doi: 10.1098/rspa.1928.0091.
[32] B. D. O'Shea, G. Andonian, S. K. Barber, C. I. Clarke, P. D. Hoang, M. J. Hogan, B. Naranjo, O. B. Williams, V. Yakimenko, and J. B. Rosenzweig, "Conductivity induced by high-field terahertz waves in dielectric material," *Phys. Rev. Lett.*, vol. 123, no. 13, Sep. 2019, doi: 10.1103/PhysRevLett.123.134801.
[33] D. Bar-Lev and J. Scheuer, "Plasmonic metasurface for efficient ultrashort pulse laser-driven particle acceleration," *Phys. Rev. Special Topics Accel. Beams*, vol. 17, no. 12, Dec. 2014, Art. no. 121302, doi: 10.1103/PhysRevLett.123.134801.
[34] P. Chen and R. J. Noble, "A solid state accelerator," in *Proc. AIP Conf.*, 1987, pp. 1–7, doi: 10.1063/1.36458.
[35] D. S. Gemmell, "Channeling and related effects in the motion of charged particles through crystals," *Rev. Modern Phys.*, vol. 46, no. 1, pp. 129–227, Jan. 1974, doi: 10.1103/RevModPhys.46.129.
[36] T. C. Chiou and T. Katsouleas, "High beam quality and efficiency in plasma-based accelerators," *Phys. Rev. Lett.*, vol. 81, no. 16, pp. 3411–3414, Oct. 1998, doi: 10.1103/PhysRevLett.81.3411.
[37] S. Gessner, E. Adli, J. M. Allen, W. An, C. I. Clarke, C. Clayton, S. Corde, J. P. Delahaye, J. Frederico, and S. Z. Green, "Demonstration of a positron beam-driven hollow channel plasma wakefield accelerator," *Nature Commun.*, vol. 7, pp. 1–6, Jun. 2016, doi: 10.1038/ncomms11785.
[38] A. A. Sahai, "Quasimonoenergetic laser plasma positron accelerator using particle-shower plasma-wave interactions," *Phys. Rev. Accel. Beams*, vol. 21, no. 8, Aug. 2018, Art. no. 081301, doi: 10.1103/PhysRevAccelBeams.21.081301.
[39] A. A. Sahai, T. Tajima, and V. D. Shiltsev, "Schemes of laser muon acceleration: Ultra-short, micron-scale beams," *Int. J. Modern Phys. A*, vol. 34, no. 34, Dec. 2019, Art. no. 1943008, doi: 10.1142/S0217751X19430085.
[40] W. K. H. Panofsky and W. A. Wenzel, "Some considerations concerning the transverse deflection of charged particles in radio-frequency fields," *Rev. Sci. Instrum.*, vol. 27, no. 11, p. 967, Nov. 1956, doi: 10.1063/1.1715427.
[41] *General Particle Tracer (GPT) Code, Pulsar Physics*. Accessed: Jul. 18, 2022. [Online]. Available: http://www.pulsar.nl/gpt/index.html
[42] *Lucretia, MATLAB Particle Tracking Code*. Accessed: Jul. 18, 2022. [Online]. Available: https://www.slac.stanford.edu/accel/ilc/codes/Lucretia/
[43] R. Talman, "Novel relativistic effect important in accelerators," *Phys. Rev. Lett.*, vol. 56, no. 14, pp. 1429–1432, Apr. 1986, doi: 10.1103/PhysRevLett.56.1429.
[44] *Handbook of Accelerator Physics and Engineering*, 2nd ed., Bunch Compress., World Sci., Singapore, 2013, doi: 10.1142/8543.
[45] J. K. Lim, P. Frigola, G. Travish, J. B. Rosenzweig, S. G. Anderson, W. J. Brown, J. S. Jacob, C. L. Robbins, and A. M. Tremaine, "Adjustable, short focal length permanent-magnet quadrupole based electron beam final focus system," *Phys. Rev. Special Topics Accel. Beams*, vol. 8, no. 7, Jul. 2005, Art. no. 072401, doi: 10.1103/PhysRevSTAB.8.072401.
[46] R. K. Li and P. Musumeci, "Single-shot MeV transmission electron microscopy with picosecond temporal resolution," *Phys. Rev. Appl.*, vol. 2, no. 2, Aug. 2014, Art. no. 024003, doi: 10.1103/PhysRevApplied.2.024003.
[47] M. Borland, "Elegant: A flexible SDDS-compliant code for accelerator simulation," Adv. Photon Source, LS-287, Argonne Nat. Lab., Lemont, IL, USA, Tech. Rep. APS-1418218, Sep. 2000. [Online]. Available: https://www.aps.anl.gov/files/APS-sync/lsnotes/files/APS_1418218.pdf

AAKASH AJIT SAHAI received the bachelor's degree (Hons.) from Pondicherry University, India, in 2003, the M.S. degree in electrical engineering from Stanford University, in 2005, the M.S. degree in physics from Indiana University Bloomington, IN, USA, in 2015, and the Ph.D. degree from Duke University, Durham, NC, in 2015. He started his research initiative focused on PetaVolts per meter plasmonics at the University of Colorado Denver (CU Denver), after being a Research Associate with the Physics Department, Imperial College London, from 2015 to 2018. The PV/m plasmonics initiative being pioneered by him at CU Denver has wide-ranging applicability cutting across high-energy physics, novel accelerators, and light-sources to affordable fusion energy alternatives. His research also focuses on innovations in compact, tunable positron, and muon sources using laser-driven plasmas. He was awarded the University Gold Medal for his bachelor's degree from Pondicherry University.

MARK GOLKOWSKI (Member, IEEE) received the B.S. degree in electrical engineering from Cornell University, Ithaca, NY, USA, in 2002, and the M.S. and Ph.D. degrees in electrical engineering from Stanford University, Stanford, CA, USA, in 2004 and 2009, respectively. He was a Postdoctoral Research Fellow with the Space, Telecommunications, and Radio Science Laboratory, Department of Electrical Engineering, Stanford University, from 2009 to 2010. He is currently a Professor with the Department of Electrical Engineering, University of Colorado Denver. He was a recipient of the National Science Foundation CAREER Award, in 2013.

THOMAS KATSOULEAS (Fellow, IEEE) received the bachelor's degree and the Ph.D. degree in physics from the University of California at Los Angeles (UCLA), in 1979 and 1984, respectively. He remained at UCLA, before joining as the Faculty Member of the University of Southern California, in 1991. In 2008, he became the Dean of the Duke University Pratt School of Engineering, and beginning in 2015, the Provost and the Executive Vice President of the University of Virginia. In 2019, he was named as the President of the University of Connecticut (UConn). Stepping down in 2021, he continues as a Professor in electrical and computer engineering at UConn.

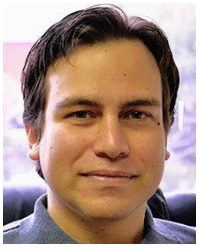

GERARD ANDONIAN received the B.S., M.S., and Ph.D. degrees in physics from the University of California at Los Angeles (UCLA), Los Angeles, CA, USA, in 1999, 2001, and 2006, respectively. He is currently a Staff Research Scientist at the Particle Beam Physics Laboratory, UCLA, where he leads several experimental efforts in the area of advanced accelerators and beam dynamics using facilities at the UCLA Pegasus Laboratory, Brookhaven National Laboratory, and the Stanford Linear Accelerator Center.

GLEN WHITE received the M.S. degree in physics from Sheffield University, in 1997, and the Ph.D. degree in physics from Lancaster University, in 2000. After holding research positions at Oxford University and Queen Mary University of London, he joined the Stanford Linear Accelerator Center (SLAC) as a Staff Scientist, in 2004. He is currently the Lead Scientist at SLAC, where his work has led extreme compression of electron and positron bunches and opened up the possibility of nC beam of sub-micron bunch lengths.

CHANDRASHEKHAR JOSHI received the B.Sc. degree in nuclear engineering from the University of London, U.K., in 1974, and the Ph.D. degree in applied physics from the University of Hull, U.K., in 1978. Following a two-year stint as a Research Associate at the National Research Council of Canada, he joined as the Faculty Member at UCLA, where he has been a Professor, since 1988. His is one of the early groups that carried out experiments on using plasma-based fields for particle accelerators.

PETER TABOREK received the B.S. degree in mathematics from the Harvey Mudd College, in 1974, and the Ph.D. degree from the California Institute of Technology, in 1980. He held roles at AT&T Bell Laboratories and Texas Instruments, before joining as the Faculty Member of the University of California at Irvine, where he is currently a Professor. He is also an experimental condensed matter physicist with interest in wide variety of systems ranging from phase transitions in quantum fluids to cilia generated flows around Xenopus frog embryos.

VIJAY HARID (Member, IEEE) received the B.S. degree in electrical and computer engineering from the University of California at Santa Barbara, Santa Barbara, CA, USA, in 2009, and the M.S. and Ph.D. degrees in electrical engineering from Stanford University, Stanford, CA, USA, in 2012 and 2015, respectively. From 2015 to 2017, he was a Scientist with the Applied Physics Laboratory, Johns Hopkins University. Since 2017, he has been an Assistant Professor with the Department of Electrical Engineering, University of Colorado Denver.

JOACHIM STOHR received the B.S. degree from Bonn University, the M.S. degree from Washington State University as a Fulbright Scholar, and the Ph.D. degree in physics from the Technical University of Munich, in 1974. Before joining Stanford University as a Professor, in 2000, he worked in different capacities at the Lawrence Berkeley National Laboratory, Stanford Linear Accelerator Center, and IBM Almaden Research Center. In 2005, he was appointed as the Director of the Stanford Synchrotron Research Laboratory and subsequently was the Director of Linear Coherent Linac Source, from 2009 to 2013. In 2011, he was awarded the Davisson-Germer Prize in Atomic or Surface Physics by the American Physical Society. Since 2015, he has been an Emeritus Professor and continues to author scientific works, in particular his third book titled *The Nature of X-Rays and their Interactions with Matter*.